Current and Temperature Distributions in a PEM Fuel Cell

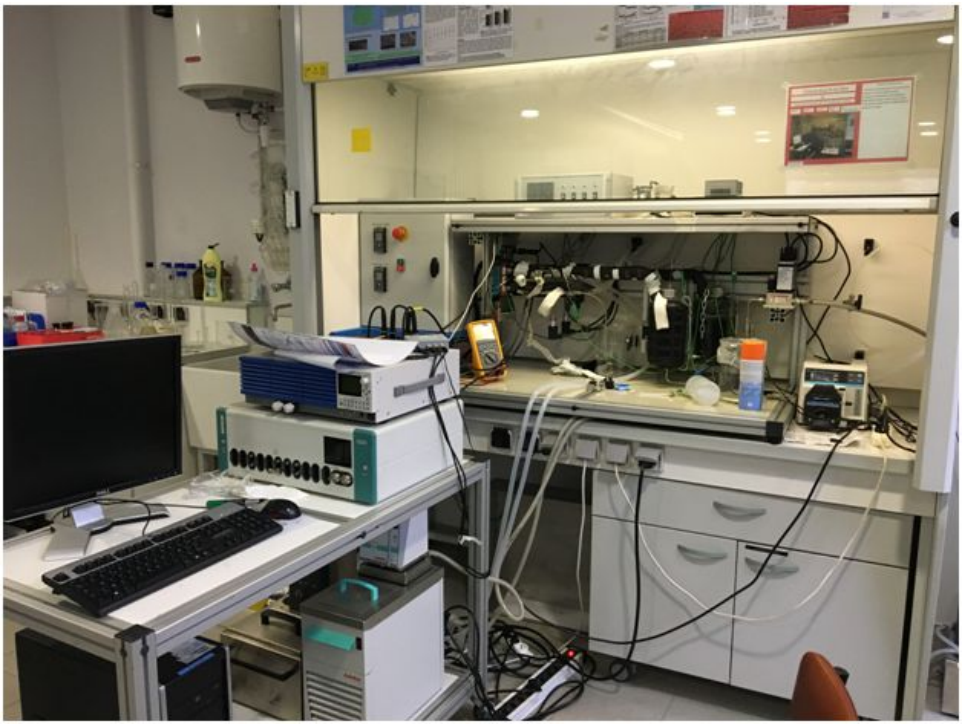

By:
Alicia Aquino
Joseph Heng

March 3rd, 2017

A Major Qualifying Project Report
Submitted to the faculty of
WORCESTER POLYTECHNIC INSTITUTE
In partial fulfilment of the requirements for the
Degree of Bachelor of Science

Submitted to:
Professor Kmiotek

Co-Advised by:
Caroline Bonnet (ENSIC)
François Lapicque (ENSIC)
Stéphane Raël (ENSIC)

Abstract

Polymer electrolyte membrane (PEM) fuel cells have attracted attention due to their relatively simple design and ability to operate at ambient pressures and low temperatures; however its commercialization is limited by low membrane durability. To improve the lifespan of the membrane, operating conditions must be optimized and effectively controlled in order to prevent operation at conditions that accelerate membrane degradation. These include nonoptimal temperature, humidity, and current conditions. In order to better understand the effect of the conditions within the fuel cell, current density and temperature distributions were measured using S++ Simulation Services's current scan shunt. After the system reached steady state, data were collected every three seconds for one minute and then analysed using MATLAB and Excel. 2D pseudocolor diagrams were plotted to compare current distributions between different current density settings and gas flow rates, between two different membranes, and between a fresh and aged membrane. Polarization and power curves and electrochemical impedance spectroscopy (EIS) were used to compare the performance between the different membranes and between the aged and fresh membrane. The results showed that current distribution was most even at a current density setting of 0.90 A/cm^2 and excess gas flow slightly increases the evenness of the current distribution. Furthermore, the results showed that current density was less evenly distributed after aging of the membrane and that the type of gas diffusion layer had an effect on the current distribution. Additional testing is recommended to verify these results.

Acknowledgements

We would like to thank Professor Stephen Kmiotek for providing us with the opportunity to work with the LRGP team at ENSIC and for supporting us throughout the project. We would also like to thank the sponsors at ENSIC, Caroline Bonnet, François Lapicque, and Stéphane Raël, for the project opportunity. We would like to express our deepest gratitude to François Lapicque for advising the project and guiding us in the right direction in order to complete the project. We would like to thank Mariem Belhadj and Divyesh Arora for their help and support in the lab. Mariem Belhadj was very kind to provide us with useful information and knowledge about the fuel cell system in the lab as well as data on the current distribution of the fuel cell when the first membrane was fresh.

Table of Contents

Table of Figures and Tables

1.0 Introduction

Polymer electrolyte membrane (PEM) fuel cells have become a research interest in the past few decades as an alternative source of energy because they are a more efficient and clean means of energy generation than the conventional burning of fossil fuels. Their simple design and low operating temperature allow for applications such as power supply to the grid, vehicles, and battery recharge. In order to make PEM fuel cells more competitive with other energy sources, the lifetime of the fuel cell must be longer than it is currently. The major factor in the aging of the fuel cell is the degradation of the membrane electrode assembly (MEA). Previous studies have shown that the degradation is related to the uneven distribution of current density in the MEA, which is affected by the flow field pattern of the bipolar plate, the composition of the MEA, and the operating conditions such as gas flow and current density settings (Lobato 2011 & Úbeda 2014). Observing how current is distributed throughout the fuel cell at various operating conditions and with different MEA compositions can provide insight on how and why the membrane degrades over time.

A possible way to predict current density distribution is to consider fuel cells as catalytic membrane reactors (Thampan, 2001) with plug flow that react hydrogen and oxygen to produce power, heat, and water. In a membrane reactor, reaction rate is highest at the inlet, where the partial pressures of the reactants are highest, and decreases as gases continue to be consumed along the channel toward the outlet of the reactor. Because the current produced by the fuel cell is proportional to the reaction rate, current density is expected to decrease from the inlet to the outlet. Understanding how to model the current density profile from the inlet to the outlet could help explain why fuel cell performance decreases over time.

Another important factor in fuel cell performance is water management, which is affected by the local temperature. High temperatures can cause drying of the membrane while low temperatures can cause condensation in the membrane. Both of these conditions accelerate membrane degradation. Therefore, analyzing temperature distribution and finding any possible correlations between the current and temperature distribution throughout the fuel cell may indicate changes in performance at certain areas of the fuel cell.

2.0 Background

2.1 Basic Principles of Fuel Cells

A fuel cell is a device that converts chemical energy contained within gases into usable electrical energy. The reaction is often irreversible and the fuel cell will operate continuously as long as reactants are supplied. The well-known benefit of this method is that it avoids the Carnot limitations associated with conventional combustion engines. Theoretically, this means that fuel cells can be designed to have very high efficiencies. Furthermore, the only byproduct of this process is water, so fuel cells have little to no environmental impact. These aspects make fuel cells a promising technology for energy production.

2.1.1 Electrochemistry

The reaction that occurs within hydrogen fuel cells is the reverse of electrolysis: hydrogen and oxygen gases react to form water and an electrical current is produced.

$$2H_2 + O_2 \rightarrow 2H_2O + \text{electricity} + \text{heat}$$

A catalyst, often platinum, is necessary in order to lower the activation energy to increase reaction rate. A diagram of an acid electrolyte fuel cell is shown in **Figure 2-1a** and the morphology of the catalyst is shown in **Figure 2-1b**.

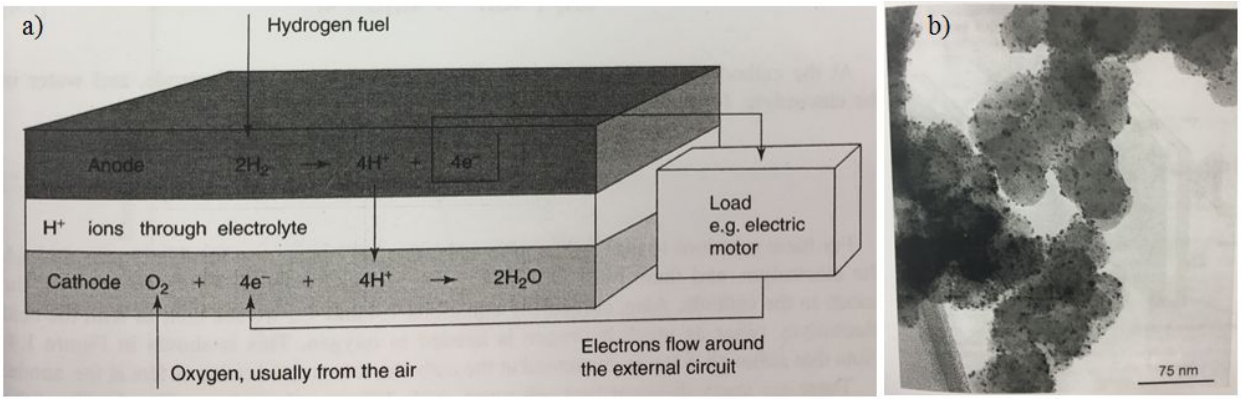

Figure 2-1: a) Diagram of an acid electrolyte fuel cell. b) TEM image of fuel cell catalyst. Taken from Larminie, 2003 (Figures 1.3 and 1.6).

This reaction is carried out within an electrochemical cell where hydrogen gas ionises into electrons and protons in an oxidation reaction in the anode and oxygen reacts with the ions to form water in a reduction reaction in the cathode.

$$2H_2 \rightarrow 4H^+ + 4e^- \qquad \text{anode}$$
$$O_2 + 4e^- + 4H^+ \rightarrow 2H_2O \qquad \text{cathode}$$

Without transfer of the electrons and hydrogen ions from the anode to the cathode, the reaction cannot proceed continuously. Electrons produced in the anode are directed through an electrical circuit to reach the cathode and hydrogen ions are passed through an acid electrolyte. The transfer of the electrons through the circuit produces current that can be used as electrical energy. Hydrogen ions may also be transferred through polymers that contain mobile hydrogen ions. These materials are called proton exchange membranes (PEM) and will be discussed further in Section 2.2.

2.1.2 Fuel Cell Design

Two components that make up the fuel cell are the membrane electrode assembly (MEA) and the bipolar plates. The assembly of the fuel cell is shown in **Figure 2-2**.

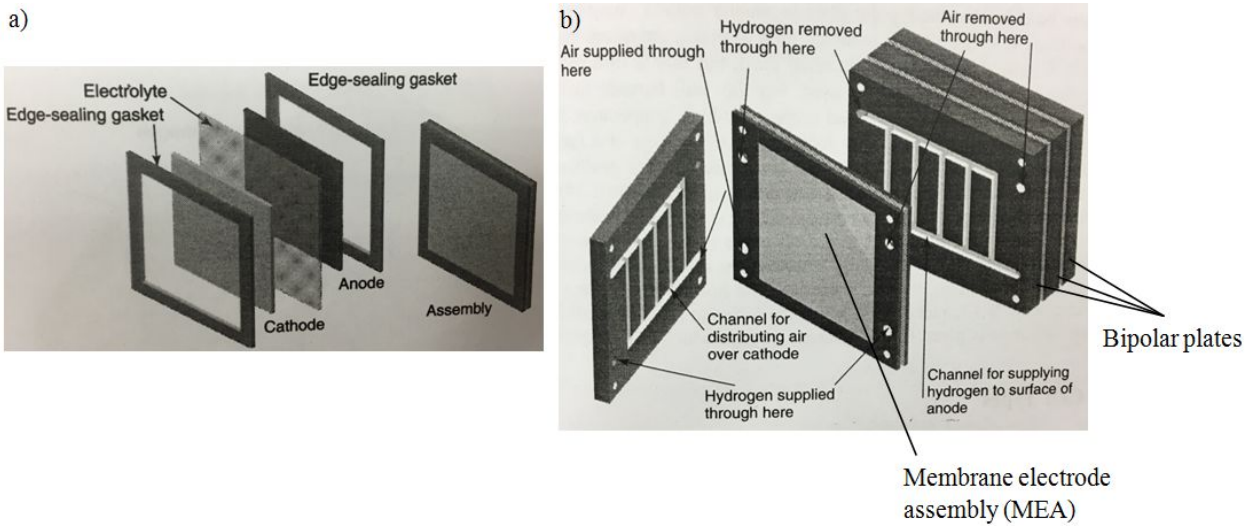

Figure 2-2: Structure of fuel cell showing a) membrane electrode assembly (MEA) and b) internal manifolding of bipolar plates. Figures taken from Larminie, 2003 (Figures 1.11 and 1.14). Bipolar plates and MEA were labeled separately and are not part of the original textbook figures.

Membrane Electrode Assembly (MEA)

The MEA consists of the anode, cathode, electrolyte, and sealing gaskets, as shown in **Figure 2-2a**. The electrolyte is positioned in between the anode and cathode to create the electrochemical cell and sealing gaskets are used to prevent leakage of gases through the porous electrodes.

The electrodes are composed of an inert carbon-based porous material to allow for efficient distribution of gases throughout the electrode. These porous electrodes are called the gas diffusion layer (GDL). On the surface of the carbon support are nano-sized platinum deposits, as shown in **Figure 2-1b**, that act as the catalyst. The porosity of the carbon support increases the surface area of the electrode in order to increase reactant, electrode, and electrolyte contact. The coming together of these three components is called three phase contact, a concept that is important in maximizing the rate of reaction.

Bipolar Plate

To increase the amount of electricity produced by a fuel cell device, many fuel cells are connected in series, as shown in **Figure 2-2b**. To do this effectively, a bipolar plate is used. A bipolar plate is multifunctional; it conducts electrical current between cells, distributes hydrogen and oxygen to the anode and cathode respectively, removes excess heat, and prevents leakage of gases and coolant. There are many variations of the bipolar plate design, which include different flow field patterns (**Figure 2-3**) and different materials of construction.

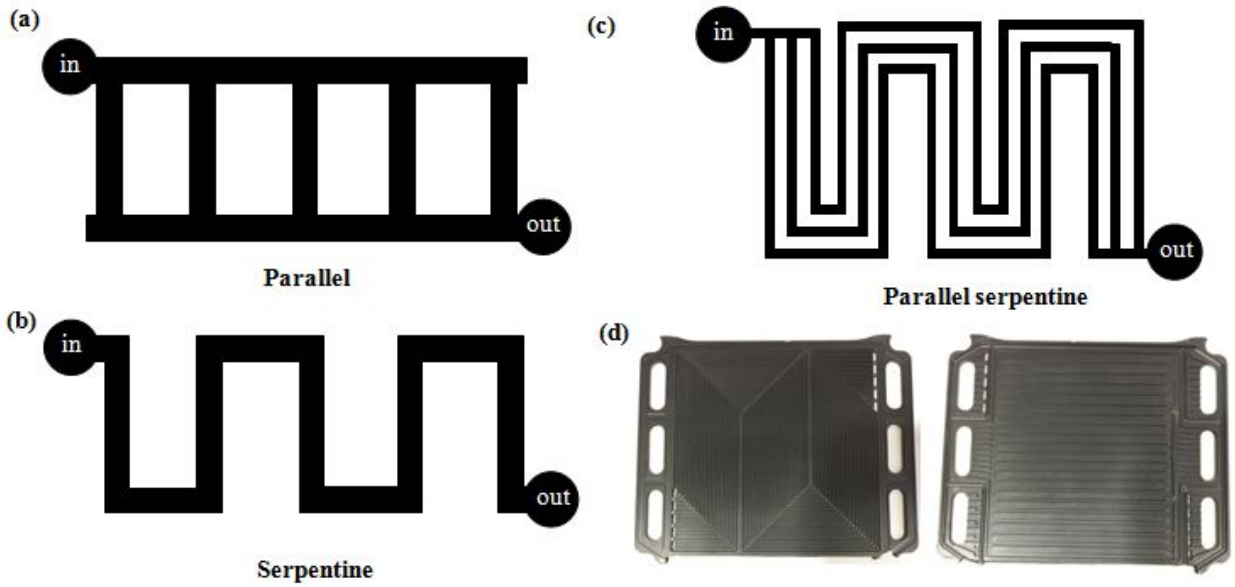

Figure 2-3: Bipolar plate flow field patterns in fuel cells: a) parallel pattern, b) serpentine pattern, c) parallel serpentine pattern, d) ENSIC bipolar plate with serpentine pattern (two sides of same plate).

A simple bipolar plate flow field pattern is the parallel grooves pattern (**Figure 2-3a**). A potential problem with this design is that water or impurities will get trapped within one of the channels. This will create a blockage that could limit the flow of gases to the blocked area, leaving an area

of the fuel cell without reactants. The serpentine design (**Figure 2-3b**) seeks to overcome this problem by creating only one path of flow. The problem with this design is that excessive work must be done to push the gases through the channel. The parallel serpentine pattern (**Figure 2-3c**) seeks to find a balance between the two designs. These are just a few examples of flow field patterns and there are many more in the literature.

The bipolar plate material must be conductive, suitable for machining, and corrosion-resistant, so are generally made from graphite and other compact carbon-based materials. Bipolar plates account for about 80% of the mass of the fuel cell, and thus also account for a high proportion of fuel cell cost (Larminie 2003). The design of the bipolar plate is an important aspect of fuel cell design.

2.1.3 Types of Fuel Cells

There are several different types of fuel cells that have varying operating conditions and materials, which allows for different uses and applications. **Table 2-1** describes the operating conditions and materials of each type of fuel cell.

	Solid Oxide Fuel Cells (SOFC)	Molten Carbonate Fuel Cells (MCFC)	Proton Exchange Membrane Fuel Cells (PEMFC)	Phosphoric Acid Fuel Cells (PAFC)	Direct Methanol Fuel Cells (DMFC)
Operating temperature	600 - 1000 °C	~650 °C	60 - 120 °C	190 - 200 °C	25 - 90 °C
Electrolyte	Yttria-stabilized ZrO_2	Li_2CO_3; K_2CO_3	Nafion	H_3PO_4	Nafion
Anode material	Ni-ZrO_2	90% Ni, 10% Cr	Pt; Pt/C	Pt/C	Pt; Pt/C
Cathode material	Sr-doped $LaMnO_3$	Li-doped NiO	Pt; Pt/C	Pt alloy/C	Pt; Pt/C
Anode reaction	$H_2 + O^{2-} \rightarrow H_2O + 2e^-$	$H_2 + CO_3^{2-} \rightarrow H_2O + CO_2 + 2e^-$	$H_2 \rightarrow 2H^+ + 2e^-$	$H_2 \rightarrow 2H^+ + 2e^-$	$CH_3OH + H_2O \rightarrow CO_2 + 6H^+ + 6e^-$
Cathode reaction	$O_2 + 4e^- \rightarrow 2O^{2-}$	$O_2 + 2CO_2 + 4e^- \rightarrow 2CO_3^{2-}$	$O_2 + 4H^+ + 4e^- \rightarrow 2H_2O$	$O_2 + 4H^+ + 4e^- \rightarrow 2H_2O$	$(3/2)O_2 + 6H^+ + 6e^- \rightarrow 3H_2O$

Table 2-1: Comparison of different types of fuel cells (Deutschmann 2012).

The most common type of fuel cell is the proton exchange membrane fuel cell (PEMFC) because it is relatively small in size, lightweight, and easy to build. It operates with hydrogen and oxygen (or air) at a relatively low temperature range of 60°C to 120°C. Platinum is the most common catalyst to speed up the anode and cathode reactions in PEMFC. Applications for different fuel cell types is described in Section 2.5.

2.1.4 Reactant Composition

Hydrogen is the most common fuel for a fuel cell and can be obtained from processing fuel sources such as natural gas, crude oil, coal, and biomass. First, the fuel source must be processed to a primary fuel, which is the feedstock of the fuel processor. Primary fuels include natural gas, gasoline, kerosene, diesel fuel, methanol, and ethanol. Processing different fuel sources to primary fuels results in different compositions of the primary fuel. It is important to remove the sulfur compounds from the fuel because sulfur compounds can severely damage fuel cells by poisoning the catalyst, preventing hydrogen from adsorbing to the catalyst. Emission of sulfur compounds is also unsafe for the environment. Removal of these components can be costly, depending on the fuel source. Coal is not often used as a fuel source because it has high sulfur content, although coal is sometimes used if it is available at a cheap price. Out of all the primary fuels, liquid hydrocarbons produce the greatest amount of hydrogen by volume and mass.

The desulfurized fuel goes to a pre-reformer, where the hydrocarbons are cracked to smaller hydrocarbon chains ranging from C_1 to C_6. The fuel then goes to a reformer, where hydrogen is produced at high temperatures. The composition of the feed to the reformer can be characterized by the carbon-to-oxygen ratio (C/O) and the steam-to-carbon ratio (S/C). These ratios will determine how much fuel can be produced. Depending on the type of the fuel cell, different fuel qualities are required. Fuel cells such as PEMFC, DMFC, and PAFC operate at lower temperatures, so carbon monoxide must be removed from the fuels for these fuel cells because carbon monoxide can poison the catalyst similar to sulfur. Fuel cells that operate at high temperatures, such as SOFC and MCFC, do not have a limit for carbon monoxide because it is difficult for carbon monoxide to adsorb to the catalyst at high temperatures.

There are a few methods to produce hydrogen in the reformer. One of the methods is steam reforming (SR), which reacts the hydrocarbon with steam in the following endothermic reaction.

$$C_xH_y + xH_2O \rightarrow xCO + ((x+y)/2)H_2$$

This method has a long startup time as an external boiler must bring the system to an operating temperature of 750-800°C. The reaction is relatively slow, which means that it is difficult to

respond to transient load requirements and start/stop cycles. A catalyst is not required, but using one would speed up the reaction and reduce the size of the reformer. SR typically use catalysts based on Ni/NiO or Co formulations supported on materials such as magnesium alumina spinel. Another reforming method is partial oxidation (POX), which partially combusts the fuel using oxygen in the following exothermic reaction.

$$C_xH_y + (x/2)O_2 \rightarrow xCO + (y/2)H_2$$

POX does not require additional heat and has a faster reaction rate than SR, which allows for smaller reactors. Due to a lower efficiency, hydrogen production is more costly with this method. This makes POX more favorable for large-scale productions of hydrogen. A third hydrogen production method, autothermal reforming (ATR), combines SR and POX to a single unit. The exothermic reaction of POX provides the heat required for the endothermic reaction of SR. ATR has higher hydrogen production than POX and faster start-up and response time than SR, which is good for small-scale hydrogen productions.

The water-gas shift (WGS) reaction is used after the reformer to increase the amount of hydrogen and reduce the amount of carbon monoxide of the stream. Steam is used to react with the carbon monoxide in the following exothermic reaction.

$$CO + H_2O \rightarrow H_2 + CO_2$$

The WGS reactor is often split to two stages: a high-temperature shift (HTS) and a low-temperature shift (LTS). HTS usually operates at 350-400°C with a Fe-Cr based catalyst and LTS usually operates at 180-240°C with a Cu-ZnO-Al_2O_3 based catalyst. These stages combined can reduce the CO concentration to about 1% (Hartnig 2012).

2.1.5 Balance of Plant

The additional equipment necessary to control and operate the core fuel cell system is called the balance of plant (BOP). The BOP includes equipment for the control and regulation of temperature, pressure, and humidity of the gases and for the conversion and storage of electricity. Examples of BOP equipment are humidifiers, pressure regulators, cooling and heating systems, and controllers. The fuel cell itself only accounts for a small portion of the cost and space required for operation, as evident in **Figure 2-4**.

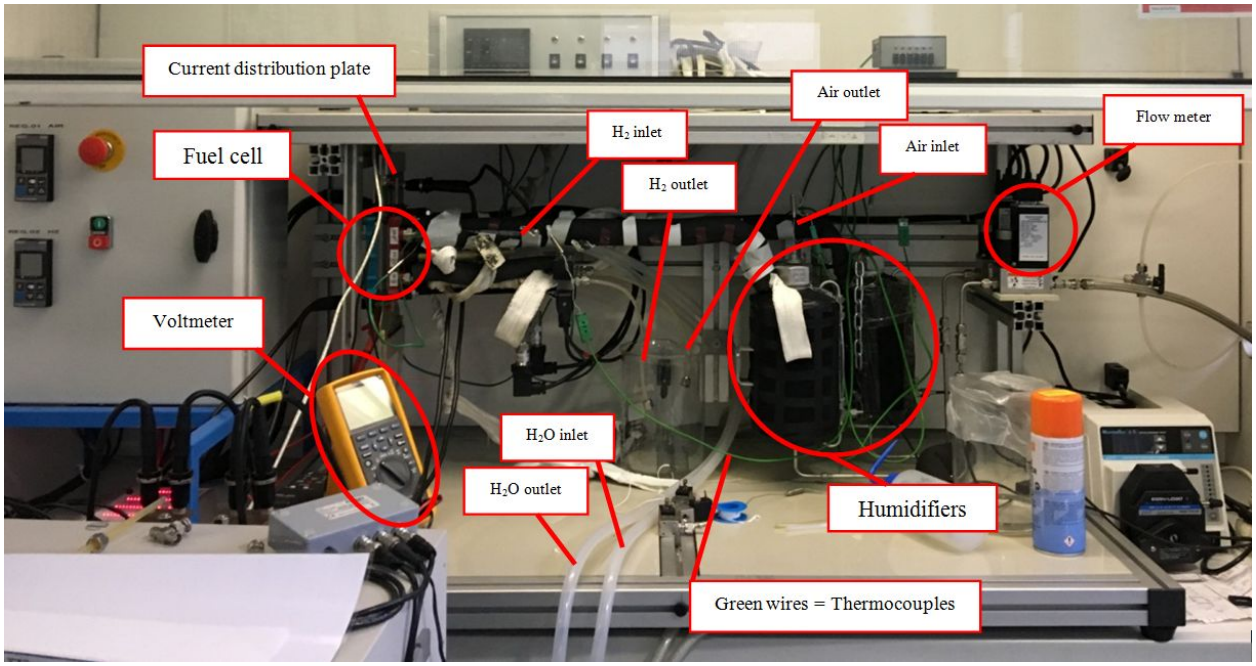

Figure 2-4: Photo of fuel cell laboratory setup in the Lapicque lab at École Nationale Supérieure des Industries Chimiques (ENSIC) in Nancy, France. Photo taken Jan. 11th, 2017.

In this setup, hydrogen and air flow from gas supplies located on the right side of the setup, not included in the photo. The gases flow through the flow meter, then through the humidifiers, and then into the fuel cell through insulated tubes. The water product leaves the fuel cell through insulated tubes into a collection beaker. Water heated by thermal baths (not included in the photo) is circulated through the fuel cell with the tubes labeled "H_2O inlet" and "H_2O outlet." There is a peristaltic pump to control the water level in the humidifiers and a pressure regulator to control the pressure of the gases at the inlet of the fuel cell. There are also thermocouples to check the temperature of the gases at certain points in the setup.

2.2 Proton Exchange Membrane Fuel Cells (PEMFC)

Proton exchange membrane fuel cells (PEMFCs) are a type of fuel cell that contains a polymer electrolyte membrane. They operate at low temperature and pressure conditions, so are well-suited for applications in transportation, portable devices, and supplementing the electric grid. A PEMFC located at École Nationale Supérieure des Industries Chimiques (ENSIC) in Nancy, France is shown in **Figure 2-5**.

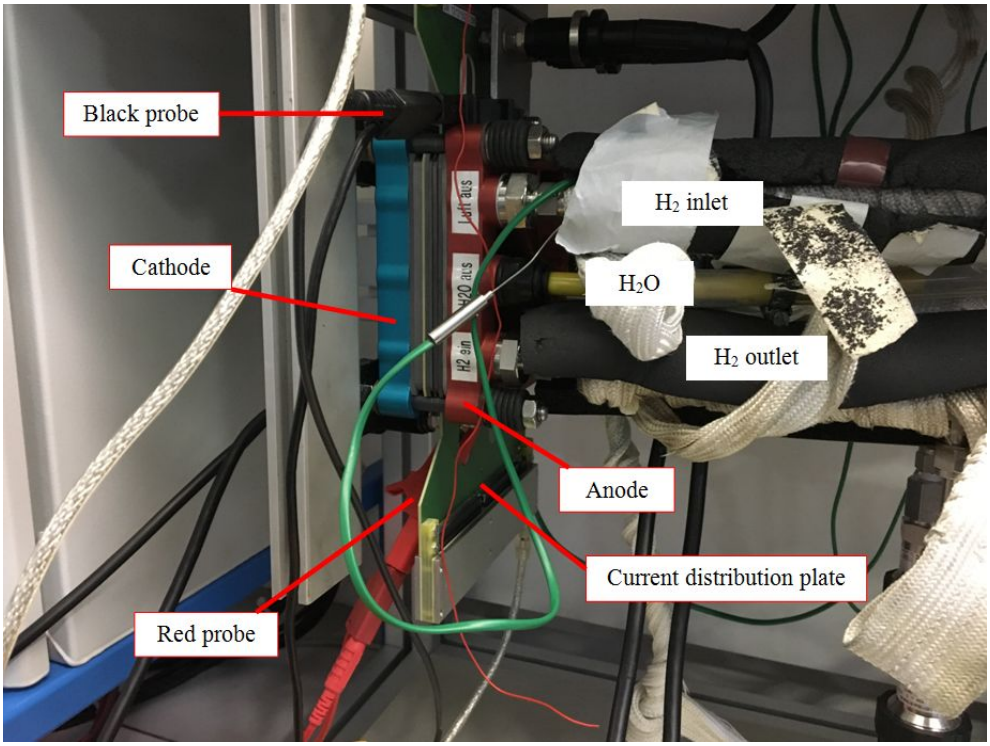

Figure 2-5: Photo of fuel cell in the Lapicque lab at École Nationale Supérieure des Industries Chimiques (ENSIC) in Nancy, France. Photo taken Jan. 11th, 2017.

2.2.1 Polymer Electrolyte Material

The industry standard polymer electrolyte material used in PEMFCs is perfluorosulfonic acid (**Figure 2-6a**) which is sold under the brand name, Nafion. The C-F bonds make the Nafion durable, resistant to chemical attack, and hydrophobic. The hydrophobicity allows Nafion to drive water out of the electrode. The sulfonated chain on Nafion, however, is very hydrophilic. This allows large quantities of water to be absorbed in areas where sulfonated regions of the Nafion molecules cluster together (**Figure 2-6b**). This is beneficial because a well-hydrated material is conductive to the flow of hydrogen ions. For this reason, Nafion is a good proton conductor and thus serves as a good electrolyte.

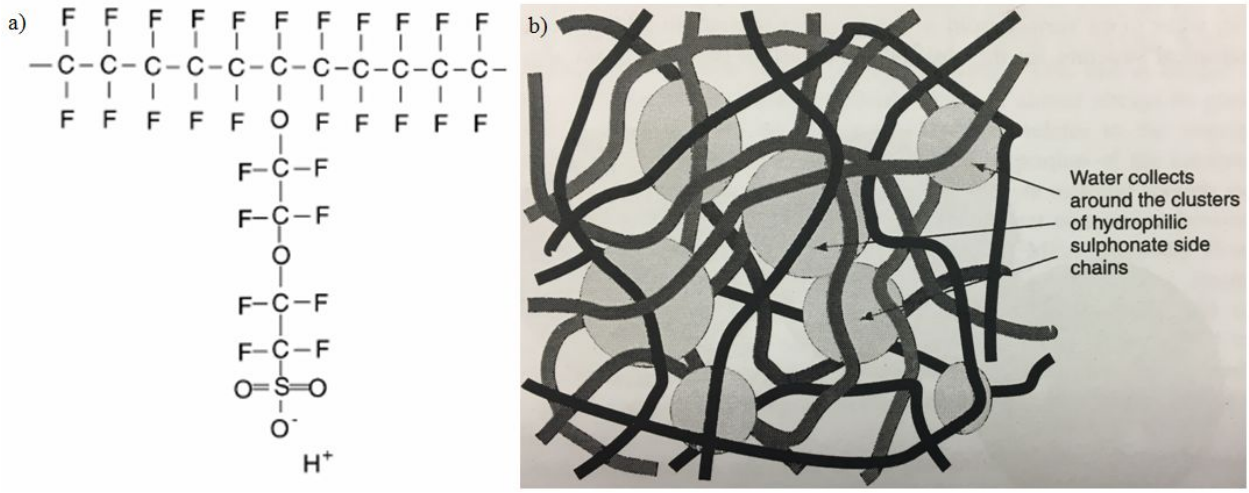

Figure 2-6: a) Structure of perfluorosulfonic acid (PTFE), or Nafion. b) Depiction of hydrated Nafion material, taken from Larminie, 2003 (Figure 4.5).

2.2.2 Water Management

Because proton conductivity of the electrolyte material is dependent on its moisture content, water management is important. Increasing moisture content will increase conductivity, but care must be given not to flood the GDL. To find this balance, the different ways that water is generated and transferred throughout the system must be considered.

Water is generated within the cathode from the reverse electrolysis reaction. Furthermore, water will be pulled from the anode to the cathode from the movement of protons through the electrolyte. This water leaves the cathode by evaporation into the circulating air that provides the oxygen fuel to the cathode. Water may also exit the cathode by diffusing back into the anode if the cathode contains more water. If not enough moisture is present on either side, a humidifier can be used to add moisture to the air or hydrogen fuel.

2.3 Current and Temperature Distribution Measurement

2.3.1 Measurement Methods

A distribution measurement plate was installed in the fuel cell at the air inlet side. It is connected to the computer through USB cables from the top and bottom of the card. This allows current and temperature distribution data to be collected through the S++ CurrentVIEW program on the computer. The fuel cell setup with the distribution measurement plate is shown in **Figure 2-7**. The next section provides a basic explanation of how the distribution measurement plate works.

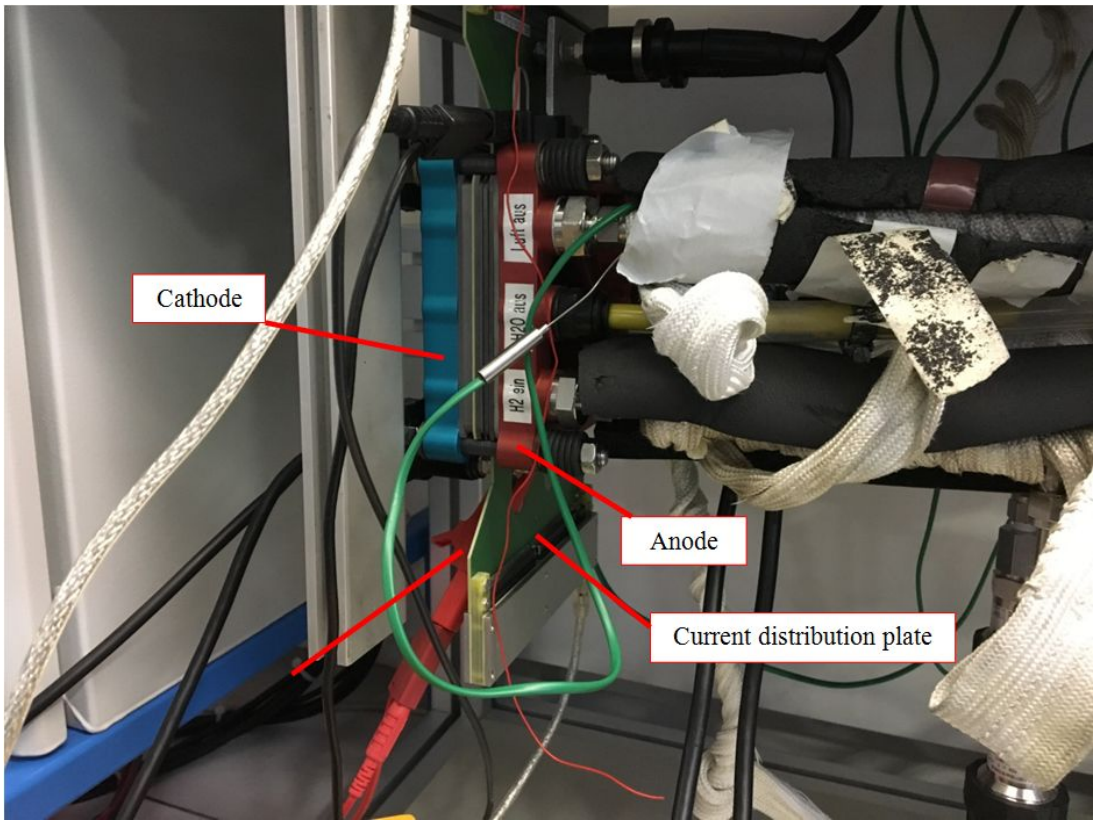

Figure 2-7: Close-up of fuel cell and distribution measurement plate.

2.3.2 Current Scan Shunt

The S++ current scan shunt measures current through shunt resistors. Shunt resistors are placed in parallel to the ammeters within the circuit and are used to divide the current between the shunt resistor and the ammeter in order to measure currents that are too high. If the resistance of the shunt resistor is known, then the current can be calculated using Ohm's law once the voltage drop across the resistor is measured. For instance, with a voltage measured at 30 mV and a resistance of 1 mOhm, the following current is calculated:

Ohm's Law: $I = V/R$, where $V = 0.03$ V and $R = 0.001$ Ohm

$I = 0.03/0.001 = 30$ A

The same method is used to calibrate a shunt resistor where a known current and voltage are used and a resistance of the shunt resistor can be calculated. Shunt resistors are designed to have low resistance in order to prevent interference with the main circuit; however the lower the resistance, the lower the resolution of the measurement is. This is because a lower resistance will result in a lower voltage drop and if the voltage drop is lower than 0.1 mV, it is more difficult to measure. From the shunt resistors the signals are directed to a multiplexer and A/D converter to

produce a digital current reading. A diagram of the current scan shunt principle is shown in **Figure 2-8**.

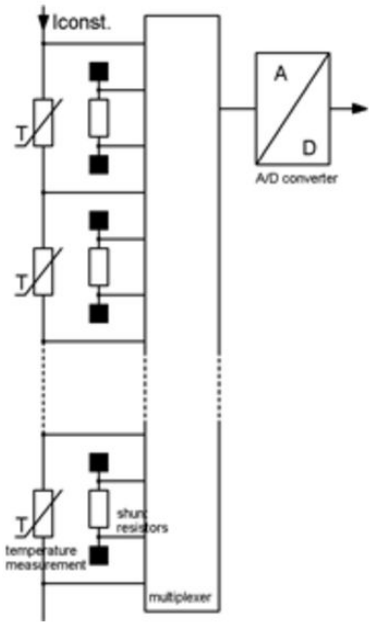

Figure 2-8: Diagram of current scan shunt principle, taken from S++ Simulations Services current scan shunt user brochure (2016 S++ Simulations Services, Vers.21.04.2016).

Using this equipment, current density and temperature distribution data over time across the fuel cell can be obtained. In the Lapicque lab the fuel cell is 100 cm^2 (10 cm x 10 cm) with 23 channels and has a serpentine flow field pattern for the gas flow plates. The diagram of the flow field pattern is shown in **Figure 2-9**.

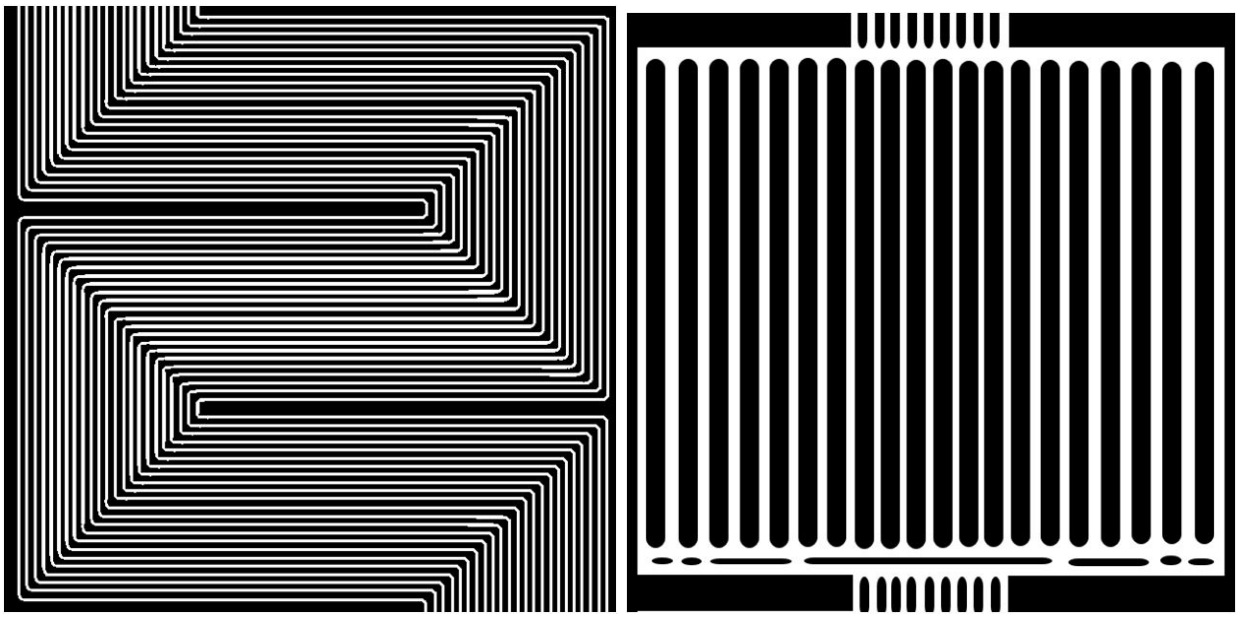

Figure 2-9: Diagram of fuel cell flow field plate on the oxygen side (left) and water side (right). Oxygen enters from top left corner of the plate and exits from the bottom right. Water flows in the opposite direction of the oxygen, entering from the bottom and exiting at the top. The plate was manufactured by ZSW, a German company.

2.4 Fuel Cell Test Methods

There are various methods to characterize the performance of a fuel cell. Each method measures different variables that determine the age of the fuel cell, or amount of degradation. The most common method is the polarization curve.

2.4.1 Polarization Curve

The polarization curve of a fuel cell system is a graph of its voltage versus current density. It shows the steady-state relationship between potential and current. A typical polarization curve is shown in **Figure 2-10**.

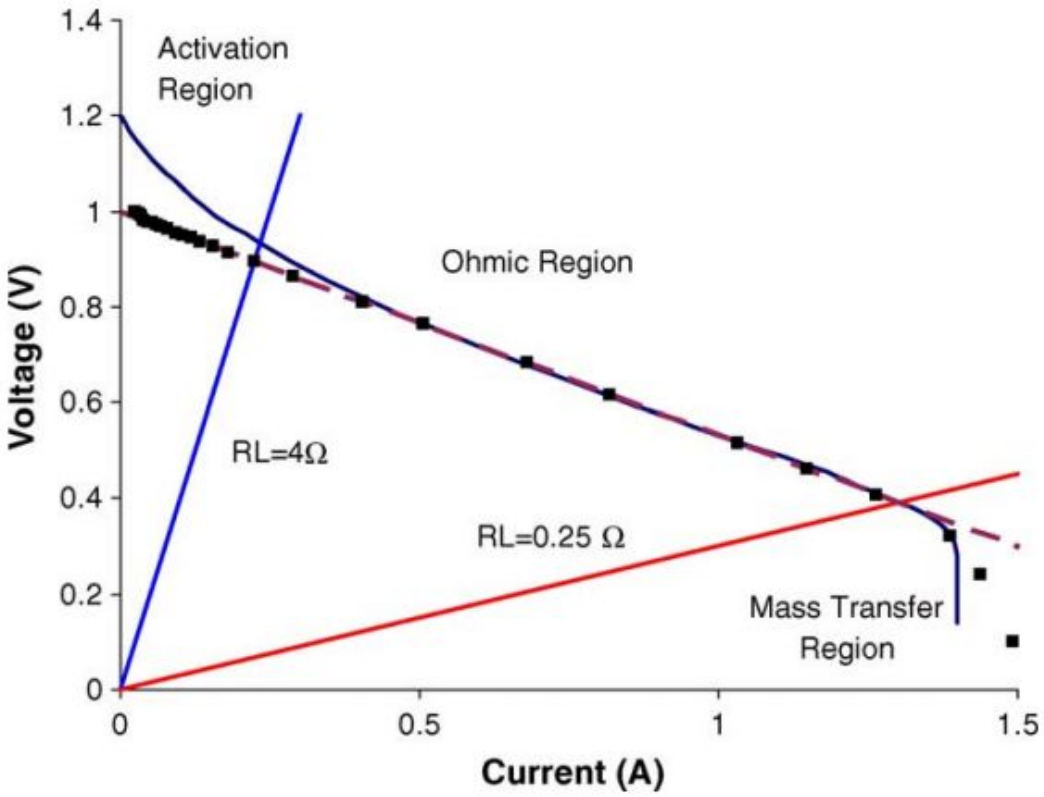

Figure 2-10: Typical polarization curve with the operating line in dark blue going through three distinct regions.

The maximum free energy of the fuel, also known as the equilibrium potential, is the theoretical maximum voltage of the system. The further away the voltage is to the theoretical maximum voltage, the lower the performance of the system. The equilibrium potential, V_0, is described by Nernst's Law.

$$V_0 = V_0^0 + RT/n_e f * \ln([Ox]/[Red])$$

There are three major regions of a polarization curve. At low current densities, the performance is dominated by kinetic losses from excess energy used to initiate the reaction, also known as activation overpotential. This is referred to as the activation polarization region or the charge transfer region. At moderate current densities, the performance is dominated by ohmic losses, which come from resistances of ionic losses in the electrodes. Ohm's law can be used to model this region, which is referred to as the ohmic polarization region.

$$\Delta\Phi = iR'$$

At high current densities, the performance is dominated by mass transfer limitations. Reactants are consumed at a faster rate than the rate of transport of the reactants. This region is known as the mass transfer limited region.

The theoretical curve of a polarization curve is the equilibrium potential subtracted by the three resistance losses, represented by the following equation:

$$V = V_0 - R * i - \frac{1}{b} * \ln\left(\frac{i}{i'_o * 10^{-4}}\right) - A * \left|\ln\left(1 - \frac{i}{i_L}\right)\right|$$

The first term, V_0 is the equilibrium potential, the second term is the ohmic losses, the third term is the charge transfer losses, and the final term is the mass transfer losses.

A variation of the polarization curve, known as the power performance curve, shown in **Figure 2-11**.

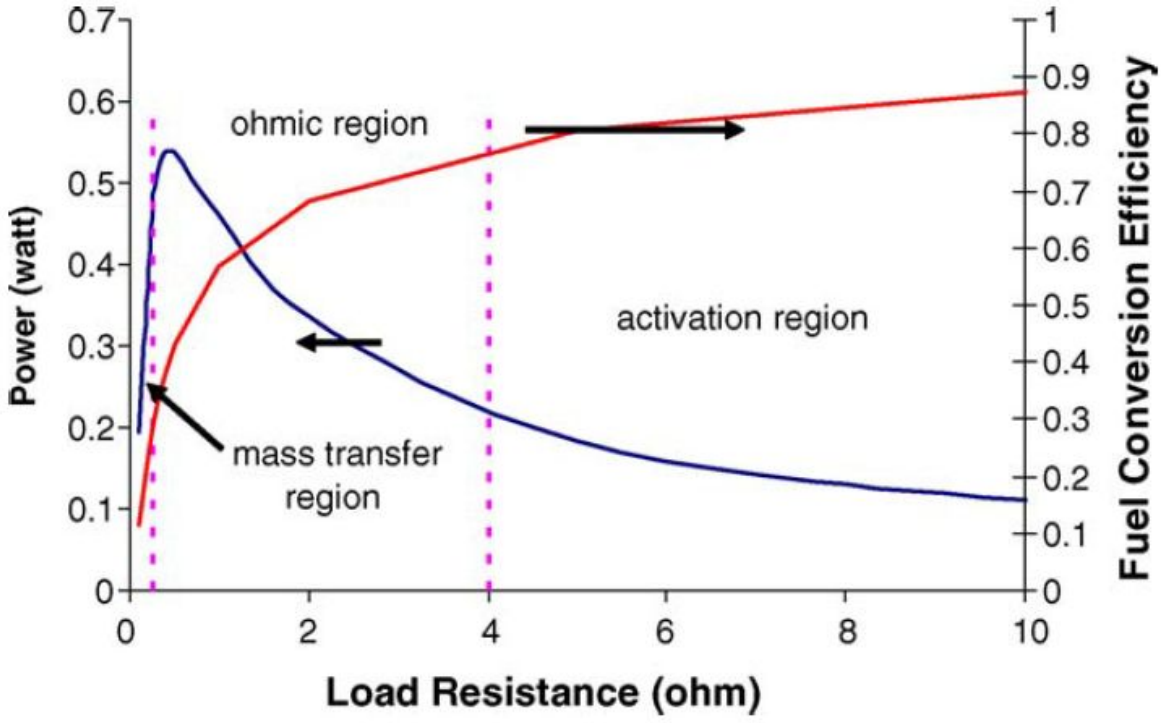

Figure 2-11: Typical power performance curve (PPC) with the operating line in dark blue going through three distinct regions. The operating line in red represents the efficiency.

The maximum power occurs when the resistance load is equal to the sum of the membrane resistance and the effective diode resistance. Fuel efficiency is 50% at the maximum power

output. The efficiency is defined as the power delivered to the external load divided by the power that would be delivered if no internal resistances existed (Benziger 2005).

$$\text{Efficiency} = (iV)/(iV_0)$$

2.4.2 Electrochemical Impedance Spectroscopy (EIS)

EIS is a technique that can be used to examine the electrochemical performance of a cell. EIS can distinguish between charge transfer resistance, ohmic resistance, and mass transfer resistance, phenomena that are illustrated in **Figure 2-12**. To do this, an alternating current (AC) is driven through the cell, the voltage is measured, and an impedance is calculated.

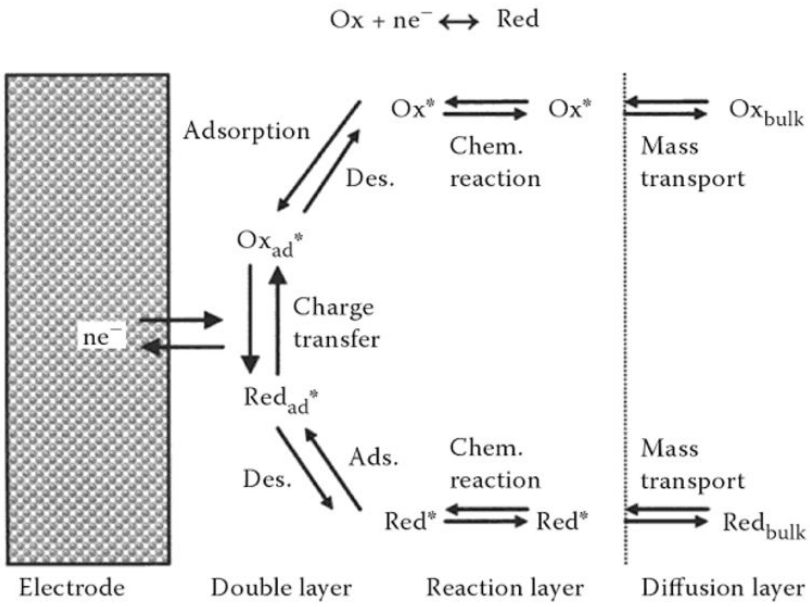

Figure 2-12: Phenomena occurring in electrochemical cell. Taken from Wang, 2011.

Impedance can then be graphed in a Nyquist plot. A Nyquist plot graphs the imaginary component of impedance versus the real component of impedance where the frequency decreases from left to right. Ohmic resistance is found from the y-axis to the intercept of the plot with the x-axis. The charge transfer resistance is represented by the first loop and the mass transfer resistance is represented by the second loop.

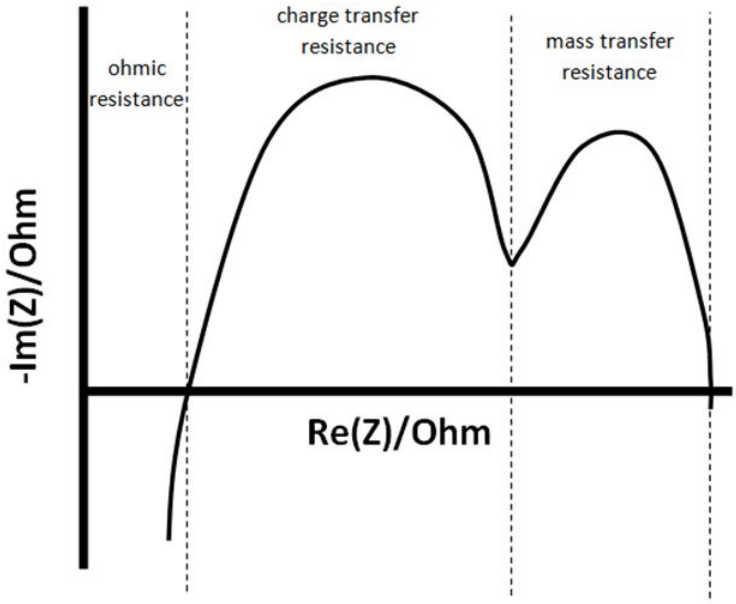

Figure 2-13: Example of Nyquist plot.

2.5 Applications

There are various applications for fuel cells of various power outputs. The most common use of fuel cells is in large-scale power plants for supply of power to the grid, which operates in the MW range. Fuel cell stacks are commercially available as DirectFuelCell® (DFC) and PureCell® which use SOFC or MCFC units. Fuel cells are also used for backup systems, in which they are coupled in parallel to the power supply and supply power or charge batteries in case of a power outage. These fuel cells are usually PEMFC and provide several kW. Electricity and heat for residential usage use SOFC. Waste heat from SOFC is used for water boiling, which has a thermal efficiency of 90%. BlueGen® is a commercial product in this field of application. Vehicles also use fuel cells in the form of Auxiliary Power Units (APU), which consists of a reformer and a fuel cell. Liquid hydrocarbons are converted to hydrogen fuel in the reformer on board in the vehicle, which is converted to electricity in the fuel cell. SOFC and MCFC are typically used for APU systems. Finally, batteries in portable electronics can be replaced by fuel cells. Currently under development, DMFC and PEMFC are used as power packs to charge electronics (Deutschmann 2012).

3.0 Methodology

The fuel cell system must be running in order to collect current density and temperature distribution data. First, hydrogen and air supplies are turned on to allow the gases to flow through the system. The thermal baths are turned on so the circulating water can be heated to about 80°C before circulating through the fuel cell. The pressure regulator is turned on to control the pressure of the gases entering the fuel cell. For the experiments performed, the pressure was maintained at 1.5 bar. The KIKUSUI electronic load is turned on to draw the current produced by the fuel cell. The Masterflex peristaltic pump is turned on at a low setting to maintain a steady water level in the humidifiers. On the computer, the dSPACE program is used to control the current setting and the flow rates of the gases through the stoichiometric factors, which are ratios of the amount of gas flowing through the system to the minimum amount of gas required for the fuel cell to operate. The S++ CurrentVIEW program is used to collect the data over time.

Current was varied using settings of 10 A, 50 A, and 90 A, corresponding to average current densities of 0.10 A/cm^2, 0.50 A/cm^2, and 0.90 A/cm^2, respectively. The stoichiometric factors of oxygen from air and hydrogen were varied using settings of 2.0, 2.5, and 3.0 for oxygen and settings of 1.2 and 2.0 for hydrogen. Four combinations of stoichiometric factors were tested: 2.0 O_2 and 1.2 H_2, 2.5 O_2 and 1.2 H_2, 3.0 O_2 and 1.2 H_2, and 3.0 O_2 and 2.0 H_2. Aside from the case of 2.0 O_2 and 1.2 H_2, data were taken when the fuel cell outlet tubes contained water droplets, which may have affected the data. When liquid droplets in the outlet air stream hinder the flow through the valve downstream of the cell, the flow was no longer continuous and steady flow, but instead was a slug flow nature. This induced transient peaks of pressure in the cell, thus, high voltage fluctuations. This phenomena preventing us from collecting additional data with smaller stoichiometries of oxygen to hydrogen. After each setting change, the fuel cell was allowed to run for 10 minutes to allow the system to reach steady state. Current distribution data were acquired from S++ CurrentVIEW in a 12x12 array and temperature distribution data were acquired simultaneously in a 6x6 array. Data were collected every three seconds for one minute and analyzed using MATLAB and Excel. For the experiments performed to compare the various operating conditions, the membrane of the fuel cell has been aged, meaning that it is near the end of its life.

Data for EIS were obtained by disconnecting the fuel cell and the S++ current scan shunt distribution measurement plate from the electronic load and connecting them to a Bio-Logic potentiostat. The EC Lab computer program was used to record the impedance for 50 points to create Nyquist plots for current settings of 5, 10, 15, 20, 30, 40, 50, 60, and 65 A.

4.0 Results

4.1 Accuracy of Data Collection Over Time

Table 4-1 shows statistical analysis of the data collected from the S++ CurrentVIEW program at current densities of 0.10, 0.50, and 0.90 A/cm^2 over time. In the table, the "Theoretical current density" column represents the ideal average current density of the 100 cm^2 plate at its respective current setting (10, 50, 90 A) assuming that the current density is evenly distributed throughout the plate and there are no losses. The "Average current density" column represents the observed average current density when every point in the 12x12 array was averaged. The "Minimum current density" column is the lowest point in the average-over-time array and the "Maximum current density" column is the highest point in the average-over-time array. These columns show how far the points in the 12x12 array deviate from the average current density value. The "Standard deviation from average" column is the standard deviation of the average-over-time array from the average current density value. The "Standard deviation/average current density" column divides the "Standard deviation from average" by the "average current density" to give a standard deviation percentage. The "Maximum standard deviation over time" shows the largest standard deviation from the average over time when comparing the corresponding points of each array of the raw data and the average over time array. The "Maximum STDEV/average current density" column takes the "Maximum standard deviation over time" and divides it by the "Average current density" and then multiplies it by 100% to show the maximum percentage of standard deviation for every individual point of the 12x12 array over time.

Theoretical current density (A/cm^2)	Average current density (A/cm^2)	Minimum current density (A/cm^2)	Maximum current density (A/cm^2)	Standard deviation from average (A/cm^2)	Standard deviation/ average current density	Maximum standard deviation over time (A/cm^2)	Maximum STDEV over time/average current density
0.10	0.10	0.04	0.15	0.02	20%	0.0011	1.1%
0.50	0.49	0.21	0.71	0.12	24%	0.0040	0.8%
0.90	0.89	0.37	1.29	0.20	22%	0.014	1.6%

Table 4-1: Statistical analysis of current distribution data obtained from S++ CurrentVIEW, based on average current over time

The average current density calculated from experimental data was found to be close to the theoretical current density that was set in dSPACE. This indicates that the current drawn from

the fuel cell is very close to the set point. The maximum standard deviation over time values were quite small, reaching at most 1.6% of the average value. This means that over time, the current read at each of the 144 locations was fairly constant. Furthermore, it was found that local current density varied widely from the average current density of the plate, with deviations averaging between 20% and 24%. This indicates a rather uneven distribution of current density in the plate.

4.2 Current Density Distribution

Twenty 12x12 arrays of current distribution over time were obtained for each parameter change. The units for the data obtained directly from the S++ CurrentVIEW program were in A/segment, so all data collected were multiplied by the conversion factor of 144 segments/100 cm^2 to obtain units of A/cm^2. Each corresponding point in the twenty arrays were averaged and a new array consisting of the average-over-time values was constructed using Excel. In order to standardize the scale for comparison between different current settings, the averaged values were divided by the theoretical average current density provided to the fuel cell (0.10 A/cm^2, 0.50 A/cm^2, or 0.90 A/cm^2) to obtain unitless values. This makes a percentage scale based on the theoretical average current density value. This means that a point with a value of 1 on the standardized scale has a value of the theoretical average current density and a point with a value of 0.5 has a value of 50% of the theoretical average current density. The standardized arrays were then inputted to MATLAB to create 2D pseudocolor plots of the current distribution. Because MATLAB plots the top row of an array at the bottom of the 2D plot and builds the plot upwards, the order of the rows obtained from Excel were reversed before entering the array into MATLAB.

To analyze these 2D pseudocolor plots, the inlet, outlet, and path of the gases must be determined. A 2D plot was superimposed onto the flow field pattern of the bipolar plate to show the inlet, outlet, and path of the gases, shown in **Figure 4-1**. These parameters will be the same for all of the 2D pseudocolor plots, but the superimposed flow field pattern will not be shown for most of the plots.

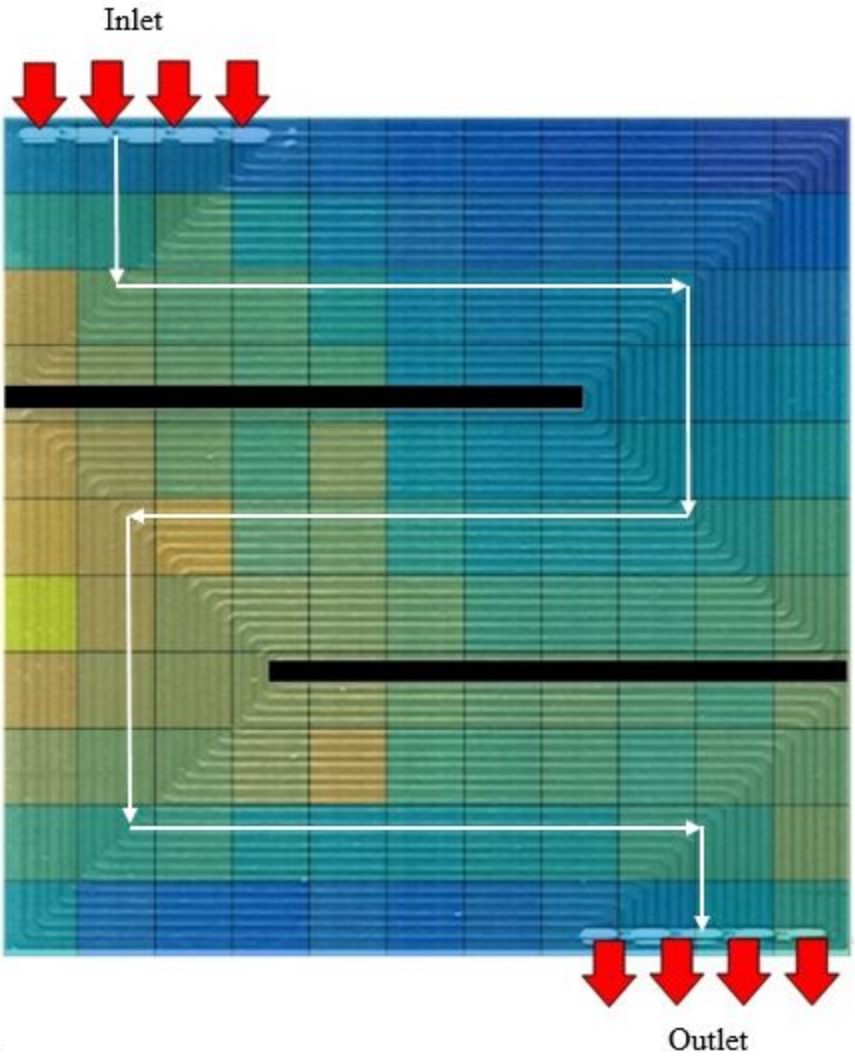

Figure 4-1: 2D pseudocolor plot superimposed on fuel cell flow field pattern so that the channels are visible. The flow plate has 23 channels arranged in a serpentine pattern. Red arrows represent inlet and outlet of gases and black rectangles outline the inner walls of the flow plate. The white arrows represent the path of the gases through the one of the channels of the serpentine pattern.

Figure 4-2 shows 2D pseudocolor plots for current distribution data collected for varying oxygen stoichiometric factors and current density settings.

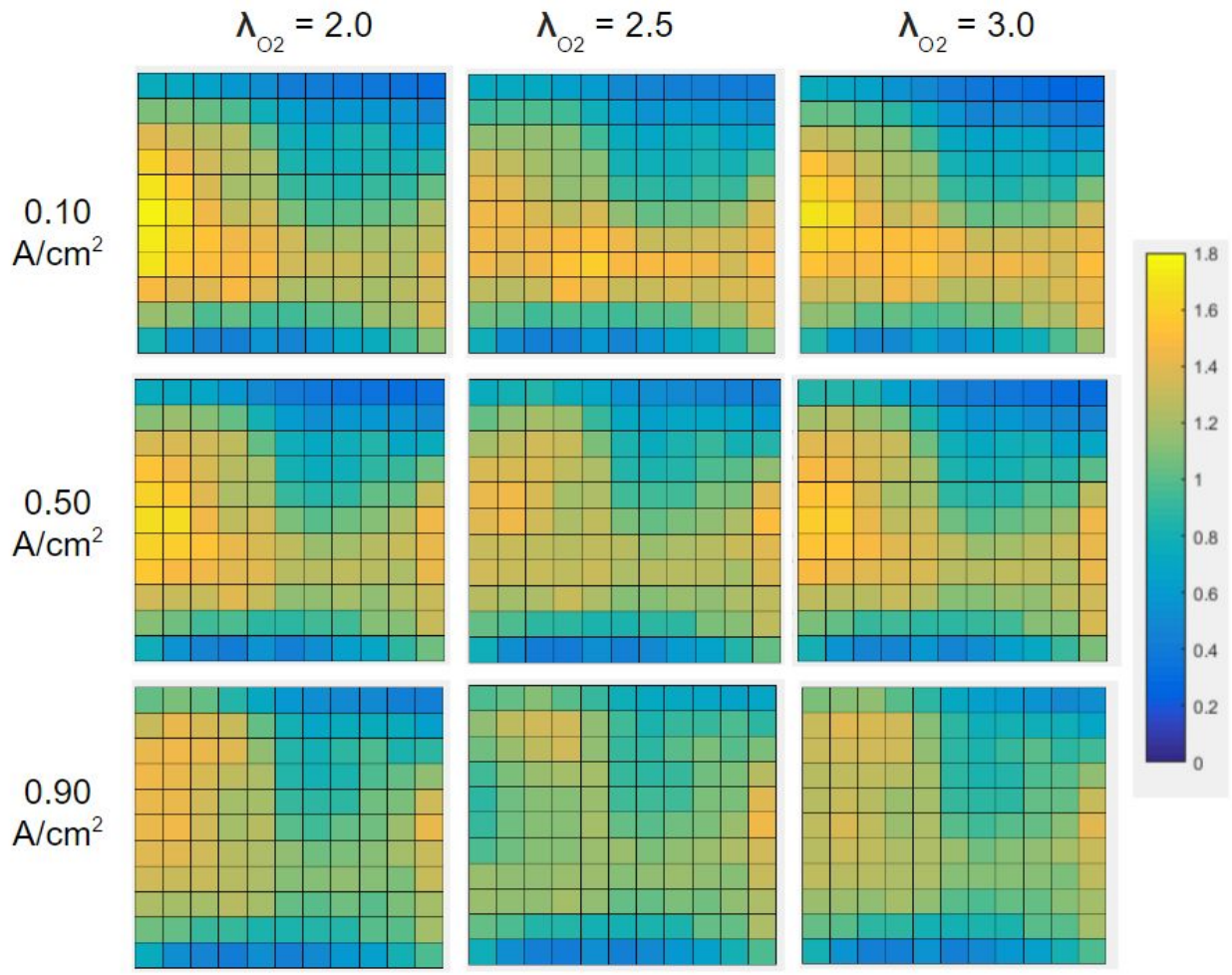

Figure 4-2: 2D pseudocolor maps of current density distribution at various current density and oxygen stoichiometric factor settings. Hydrogen stoichiometric factor is fixed at 1.2. The scale is standardized, so is the same for all plots.

These figures show that the borders along the entrance and exit of the flow plate have relatively low current density while the areas around the inner walls have the highest current density. To analyze the current distribution trends, the statistical analysis values (maximum, minimum, average, standard deviation) were calculated as the average of all three current density settings (0.10, 0.50, 0.90 A/cm^2) at each of the three oxygen stoichiometric factors (2.0, 2.5, 3.0) and vice versa. Of note is that at 0.10 A/cm^2, there are areas of high and low current density, whereas when current density increases to 0.50 A/cm^2 and 0.90 A/cm^2, current density is more evenly distributed throughout the plate. This is evident in **Table 4-2** where the standard deviation from the average current density decreases with increasing current density, the maximum standardized value decreases with increasing current density, and the minimum value is highest at 0.90 A/cm^2. In **Table 4-3**, the trend shows that the oxygen setting of 2.5 produces the most evenly distributed

current density compared to oxygen stoichiometries of 2.0 and 3.0 with the lowest standard deviation from the average, lowest maximum, and highest minimum values.

Current density (A/cm^2)	Maximum standardized value	Minimum standardized value	Average standardized value	Standard deviation from average
0.10	1.77	0.15	0.98	0.42
0.50	1.68	0.15	0.98	0.38
0.90	1.48	0.20	0.98	0.30

Table 4-2: Statistics of standardized current density data, combining the three different oxygen stoichiometry settings, at each current density setting.

O_2 stoichiometry	Maximum standardized value	Minimum standardized value	Average standardized value	Standard deviation from average
2.0	1.77	0.15	0.98	0.38
2.5	1.58	0.20	0.98	0.33
3.0	1.69	0.15	0.98	0.37

Table 4-3: Statistics of standardized current density data, combining the three different current density settings, at each oxygen stoichiometry setting.

Both tables show that the averages of standardized values for each current density or oxygen stoichiometry were equal (0.98). Theoretically, the average standardized value should be equal to 1 because this value divides the average of measured current densities by the average current density setting (0.10, 0.50, or 0.90 A/cm^2). The slight deviation from 1 indicates that the set current density is greater than the actual current density and is consistently so. Perhaps the distribution plate could be calibrated better, but it is fairly accurate and does not affect the trends and comparisons discussed in this report.

Figure 4-3 shows 2D pseudocolor plots for two different hydrogen stoichiometric factors at a constant oxygen flow rate and varying current density settings.

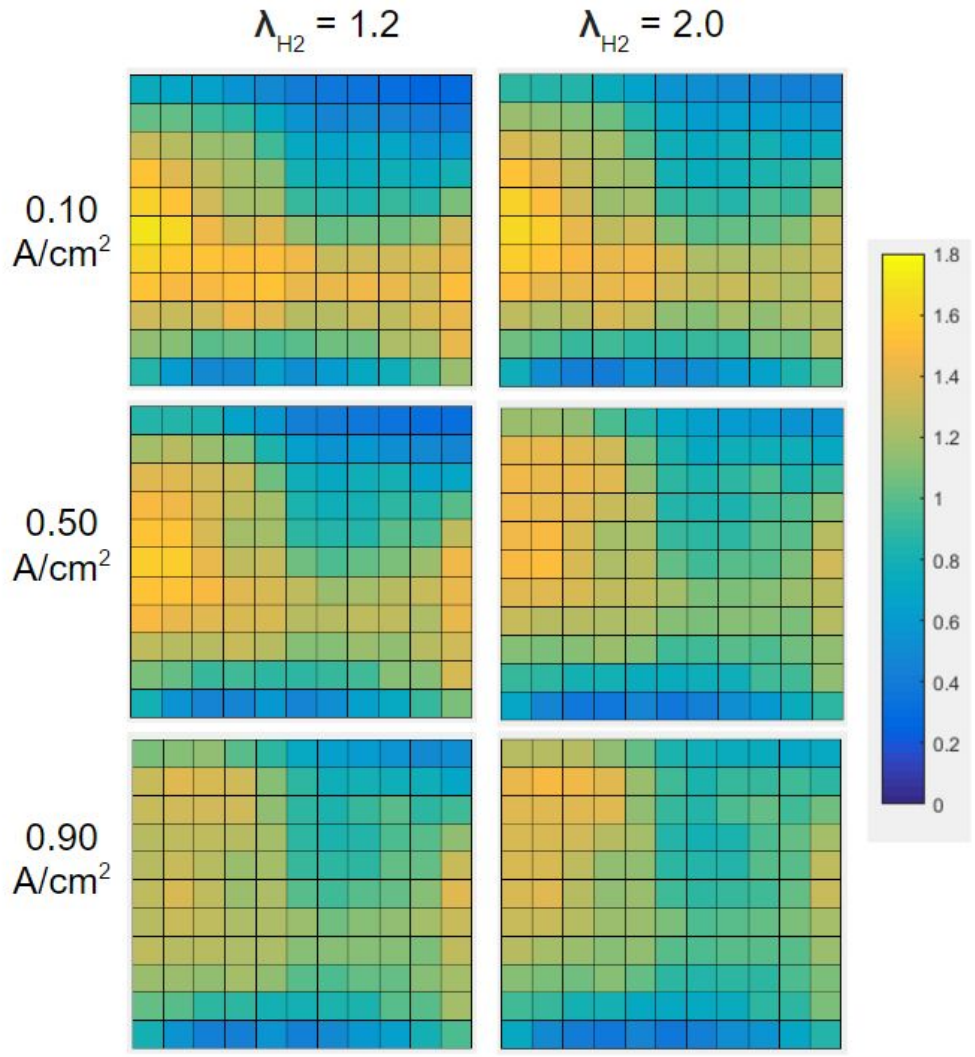

Figure 4-3: 2D pseudocolor maps of current density distribution at various current density and hydrogen stoichiometric factor settings. Oxygen stoichiometric factor is fixed at 3.0. The scale is standardized, so is the same for all plots.

H_2 stoichiometry	**Maximum standardized value**	**Minimum standardized value**	**Average standardized value**	**Standard deviation from average**
1.2	1.69	0.15	0.98	0.37
2.0	1.66	0.23	0.98	0.32

Table 4-4: Statistics of standardized current density data, combining the three different current density settings, at each hydrogen stoichiometry setting.

Table 4-4 shows that the stoichiometric factor of 2.0 for hydrogen yields a lower maximum value, a higher minimum value, and a smaller standard deviation than the stoichiometric factor of 1.2 for hydrogen, which shows that a higher flow rate of hydrogen results in a slightly more even current density distribution. From **Figure 4-3**, the higher stoichiometric factor of 2.0 yields a slightly higher current density distribution at the inlet than the lower stoichiometric factor of 1.2.

4.3 "Unfolded" View of Current Density Distribution

As an alternative way to visualize how current density is distributed throughout the plate, the serpentine pattern of the plate was rearranged into an "unfolded" view, which unfolds the bends of the serpentine pattern into a straight, continuous row of data from the inlet to the outlet. The current density profile across the unfolded rows was constructed. The constructed plot assumes that the reactants in each path travel at the same speed so each path travels from the inlet to the outlet at the same interval of time, but each path will not be vertically aligned on the plate. **Figure 4-4** shows a fuel cell plate with five paths displayed, spread out among the 23 channels of the flow field pattern. The red path will be referred to as the "top edge" of the plate, the orange path will be the "top side," the yellow path will be the "middle," the green path will be the "bottom side," and the blue path will be the "bottom edge."

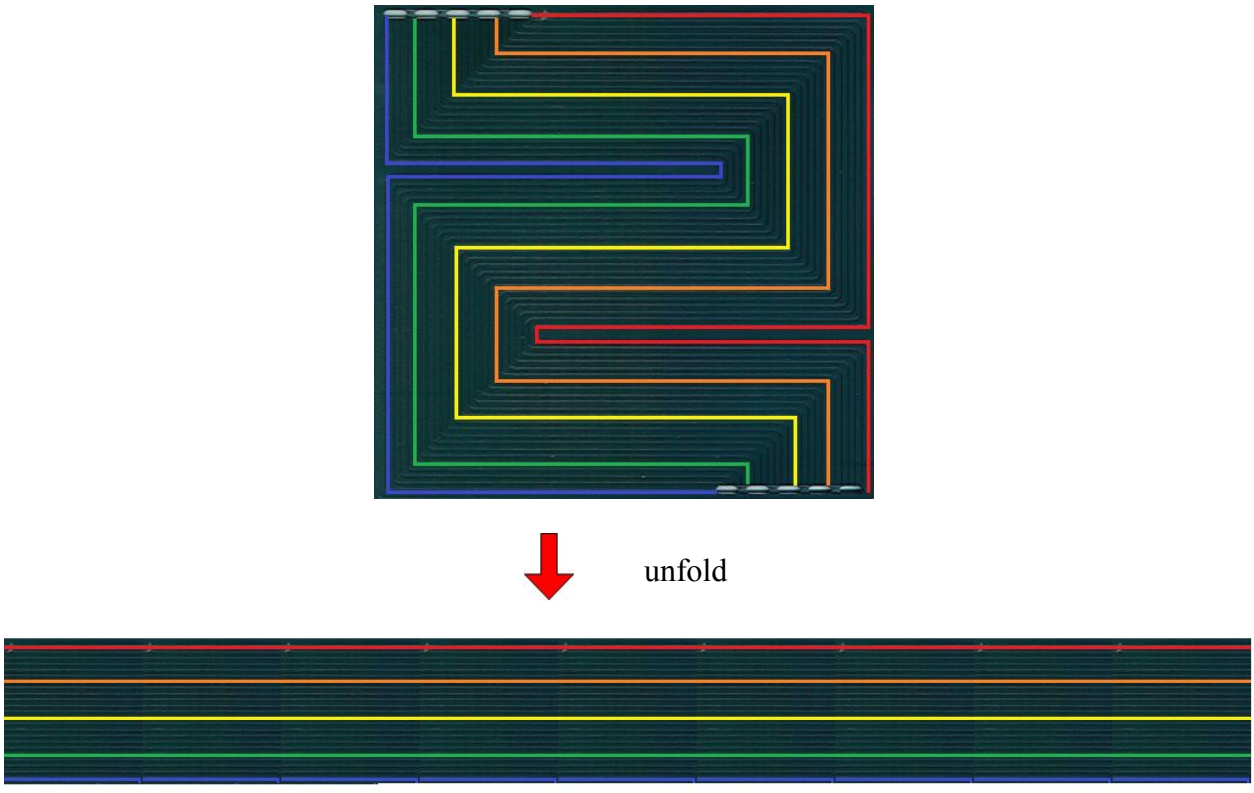

Figure 4-4: Schematic of unfolded flow plate.

Data points on these five paths were used to construct the current density profile. In order to determine which data point to use for each point on each path, the superimposed 2D plot of a 12x12 array on the flow field pattern was labeled with letters and numbers corresponding to the grid layout of Excel, shown in **Figure 4-5a**, which allowed matching of the data points on the 2D plot to the data points in Excel. For example, the point A5 on the 2D plot would correspond to the data point in the A5 cell in Excel. The positions of the data points on the 2D plot that were used for the unfolded current density profile are shown in **Figure 4-5b**.

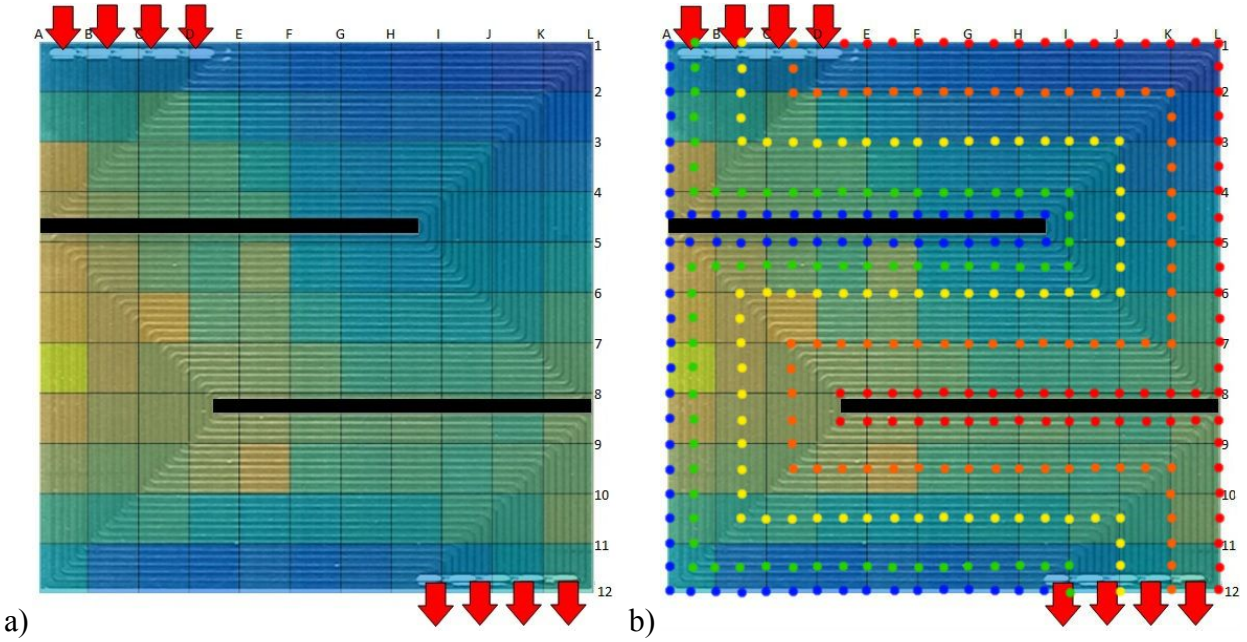

Figure 4-5: a) 2D pseudocolor plot superimposed on fuel cell flow field pattern. The positions of the data points are represented by the letter (column) and the number (row) labeled on the top and right edge of the plot. b) Exact positions of the data points used to construct an unfolded current distribution profile. The color of each path corresponds to the paths in **Figure 4-4**.

Data points that were used for the unfolded profile were taken in intervals of every half-square. The points that lie in between multiple data points were taken as averages of the data points that they lie between. For example, points on the edge of a square between two points, such as the first orange point from the inlet in **Figure 4-5b**, were taken as averages of those two points and points in the center of a square, such as the second orange point from the inlet in **Figure 4-5b**, were taken as averages of all four corner points. The top edge path begins at the top, between D1 and E1. The first data point for this path would therefore be the average of D1 and E1, or (D1+E1)/2. The next point is a half-square to the right, or point E1. The next point after that is another half-square to the right, or the point (E1+F1)/2. The path continues around the edge of the plate and around the inner serpentine boundary. The positions of the points surrounding the

serpentine boundary were rounded to the nearest half-square to simplify the process. This top edge path exits at the point L12. **Table 4-5** describes each path's inlet and outlet points. Each path consisted of 68 data points.

	Inlet Point	Outlet Point
Top edge	(D1+E1)/2	L12
Top side	(C1+D1)/2	K12
Middle	(B1+C1)/2	J12
Bottom side	(A1+B1)/2	I12
Bottom edge	A1	(H12+I12)/2

Table 4-5: Inlet and outlet points of each unfolded path used in Excel.

This data was used to construct pseudocolor plots and linearized graphs of the unfolded view of the flow field pattern to observe the differences in current distribution from the inlet to the outlet between the five paths. The pseudocolor plots for each current density setting are shown in **Figure 4-6** and the linearized graphs for each current density setting are shown in **Figures 4-7 to 4-9**. The following plots and graphs are for stoichiometric factors of 1.2 for hydrogen and 2.0 for oxygen. Additional linearized graphs were constructed for the other combinations of stoichiometric factors and can be seen in **Appendix C**.

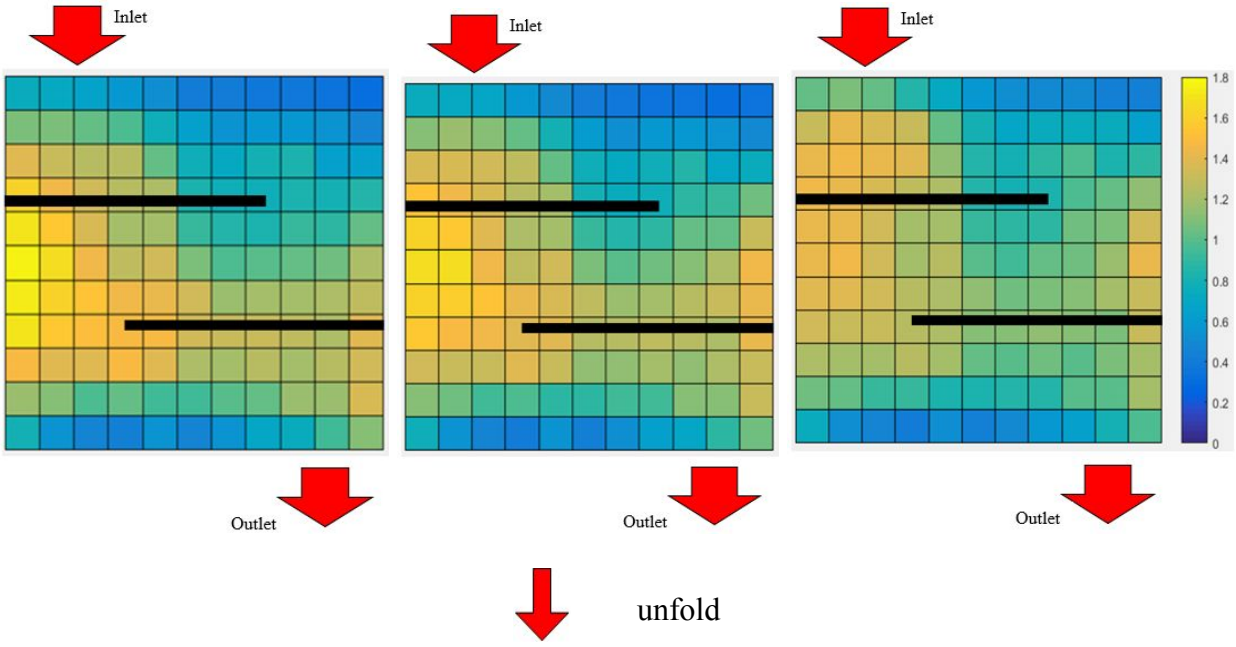

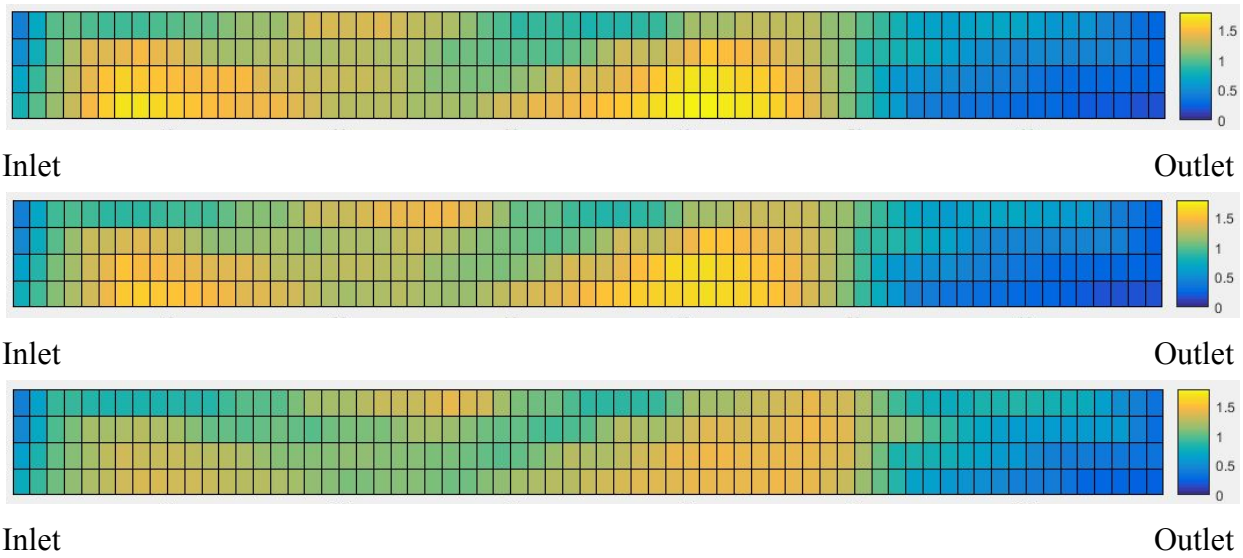

Figure 4-6: 2D pseudocolor plots of unfolded data for 0.10, 0.50, and 0.90 A/cm^2 from left to right for the 12x12 plots (top) and from top to bottom for the unfolded view (bottom). For comparison to **Figure 4-4**, the top row corresponds to the top edge (red path), the next row below it is the top side (orange path), the middle row is the middle (yellow path), the next row below it is the bottom side (green path), and the bottom row is the bottom edge (blue path).

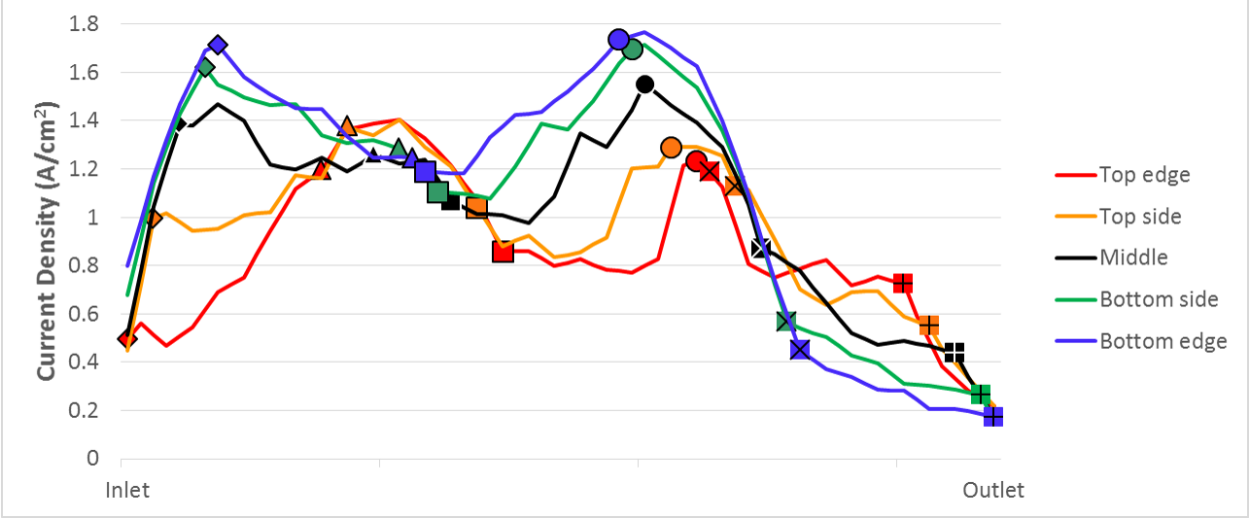

Figure 4-7: Linearized graph of unfolded data for 0.10 A/cm^2 with a standardized scale. Each marker represents a bend in the serpentine pattern, with each marker shape representing a different bend.

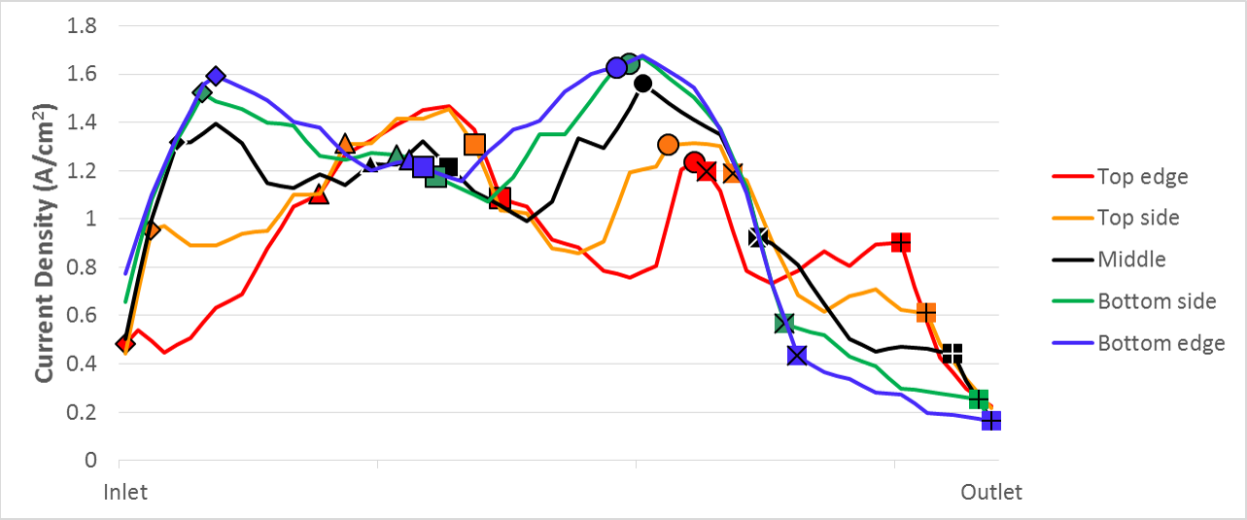

Figure 4-8: Linearized graph of unfolded data for 0.50 A/cm^2 with a standardized scale. Each marker represents a bend in the serpentine pattern, with each marker shape representing a different bend.

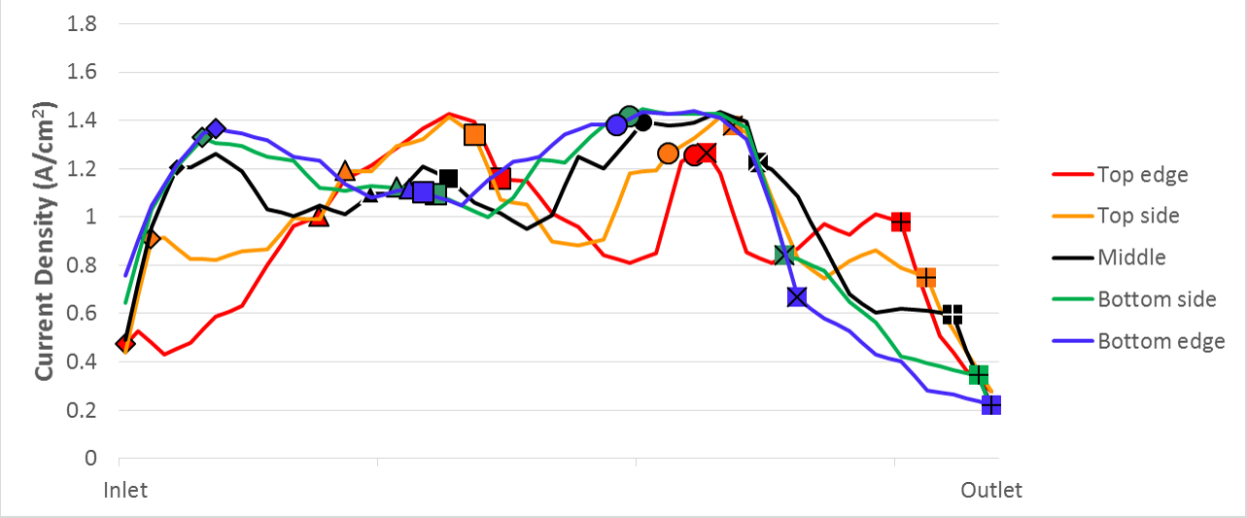

Figure 4-9: Linearized graph of unfolded data for 0.90 A/cm^2 with a standardized scale. Each marker represents a bend in the serpentine pattern, with each marker shape representing a different bend.

Because the points of the paths are not vertically aligned on the fuel cell plate, markers are included in **Figures 4-7 to 4-9** to represent a change in direction of the path. The first marker in each path is a diamond, which represents the points on the first bend near the inlet. The second marker is a triangle, representing the points on the second bend. The remaining markers, in order, are a square, a circle, a square with an X, and a square with a +. They represent the points on the next four bends of the flow field pattern.

Starting from the inlet to the first bend, the current increases to a local maximum for the middle and bottom paths. The top paths begin on the bend, so the current is at a local minimum. The middle and bottom paths then decrease to a local minimum at the next two bends, which are located very close together for these paths. For the top paths, the current increases to a local maximum at the second bend and then decreases to a local minimum at the third bend. All paths then increase to a local maximum at the fourth bend. The current density is higher at the bottom edge path than it is at the top edge path at this bend. Following the final two bends to the outlet, all paths decrease to a global minimum. The bends of the serpentine pattern are large contributors to the unevenness of current distribution. Overall, there is more current distributed to the bottom edge than the top edge.

4.4 Temperature Distribution

Temperature is an important factor in studying PEM fuel cell membrane degradation because it affects water management, proton transfer, and chemical reaction rates. These are key factors in the optimization of fuel cell performance. Temperature is controlled by the side of the bipolar plate opposite to the side of the gas flow, where there are channels for circulating water, as shown on the right image of **Figure 2-9**. These channels essentially act as a countercurrent heat exchanger where the purpose of the water is to maintain the temperature of the fuel cell.

Similar to current distribution, twenty 6x6 arrays of temperature distribution over time were obtained for each parameter change. Each corresponding point in the twenty arrays were averaged and a new array consisting of the average-over-time values was constructed using Excel. The arrays were then inputted to MATLAB to create 2D pseudocolor plots of the temperature distribution. Because MATLAB plots the top row of an array at the bottom of the 2D plot and builds the plot upwards, the order of the rows obtained from Excel were reversed before entering the array into MATLAB. For comparison between the plots at different operating conditions, the scale was fixed at a range of 74°C to 81°C because the maximum and minimum values of all data points were 80.62°C and 74.06°C, respectively. **Figure 4-10** shows the temperature averages over time plotted as 2D pseudocolor plots for varying oxygen stoichiometric factors.

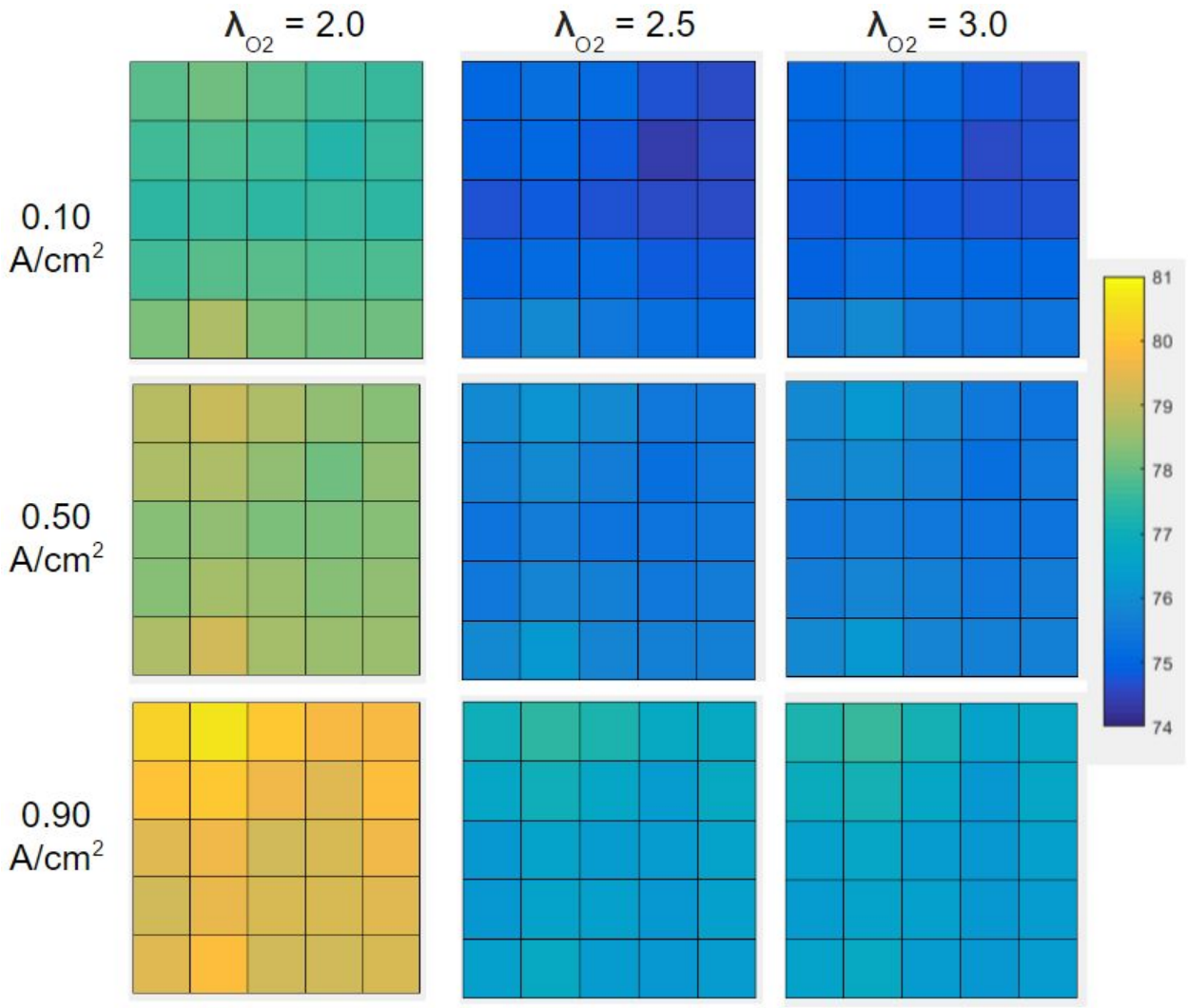

Figure 4-10: 2D pseudocolor maps of temperature distribution at various current density and oxygen stoichiometric factor settings. Hydrogen stoichiometric factor is fixed at 1.2.

When comparing temperature distribution among different current density settings at a fixed oxygen stoichiometric factor, an increase in temperature with increasing current density setting is observed. This makes sense because as current density increases, reaction rate increases. An increased reaction rate produces a proportional increase in heat generation because the reaction of oxygen and hydrogen to produce water is exothermic. Statistical analyses of this are shown in **Table 4-6**. Because the temperature distribution varies so much among the different current densities and oxygen stoichiometric ratios, perhaps the cooling and heating effect of the circulating water is not sufficient to keep the temperature both uniform and constant.

Current density (A/cm^2)	Maximum temperature (°C)	Minimum temperature (°C)	Average temperature (°C)	Standard deviation from average (°C)
0.10	78.7	74.1	75.9	1.38
0.50	79.2	75.0	76.6	1.40
0.90	80.6	76.2	77.6	1.47

Table 4-6: Temperature distribution statistics, combining the three different oxygen stoichiometric factor settings, at each current density setting.

When comparing the temperature distribution among different oxygen stoichiometric factors at fixed current density settings, it is observed that the fuel cell plate is at a relatively high temperature at an oxygen stoichiometric factor of 2.0, where the average temperature is 78.6°C, compared to at oxygen stoichiometric factors of 2.5 and 3.0, where the average temperature for both is 75.7°C. The maximum, minimum, and average temperatures of the plate at 2.5 and 3.0 oxygen stoichiometric factors are about the same, indicating no significant difference when increasing oxygen stoichiometric factor past 2.5; however standard deviation decreases as oxygen stoichiometric factor increases, indicating that increasing oxygen stoichiometric factor may produce a more even temperature distribution within the plate. These statistics are shown in **Table 4-7**.

O_2 stoichiometric factor	Maximum temperature (°C)	Minimum temperature (°C)	Average temperature (°C)	Standard deviation from average (°C)
2.0	80.6	77.1	78.6	0.83
2.5	77.5	74.1	75.7	0.77
3.0	77.5	74.3	75.7	0.73

Table 4-7: Temperature distribution statistics, combining the three different current density settings, at each oxygen stoichiometric factor setting.

The temperature distributions between the different hydrogen stoichiometric factors at the same current density settings are not significantly different. **Figure 4-11** shows that peaks in temperature occur in the same general area for hydrogen stoichiometric factors of 1.2 and 2.0. Statistics in **Table 4-8** show that temperature averages and ranges are nearly identical when comparing the two stoichiometric factors of hydrogen.

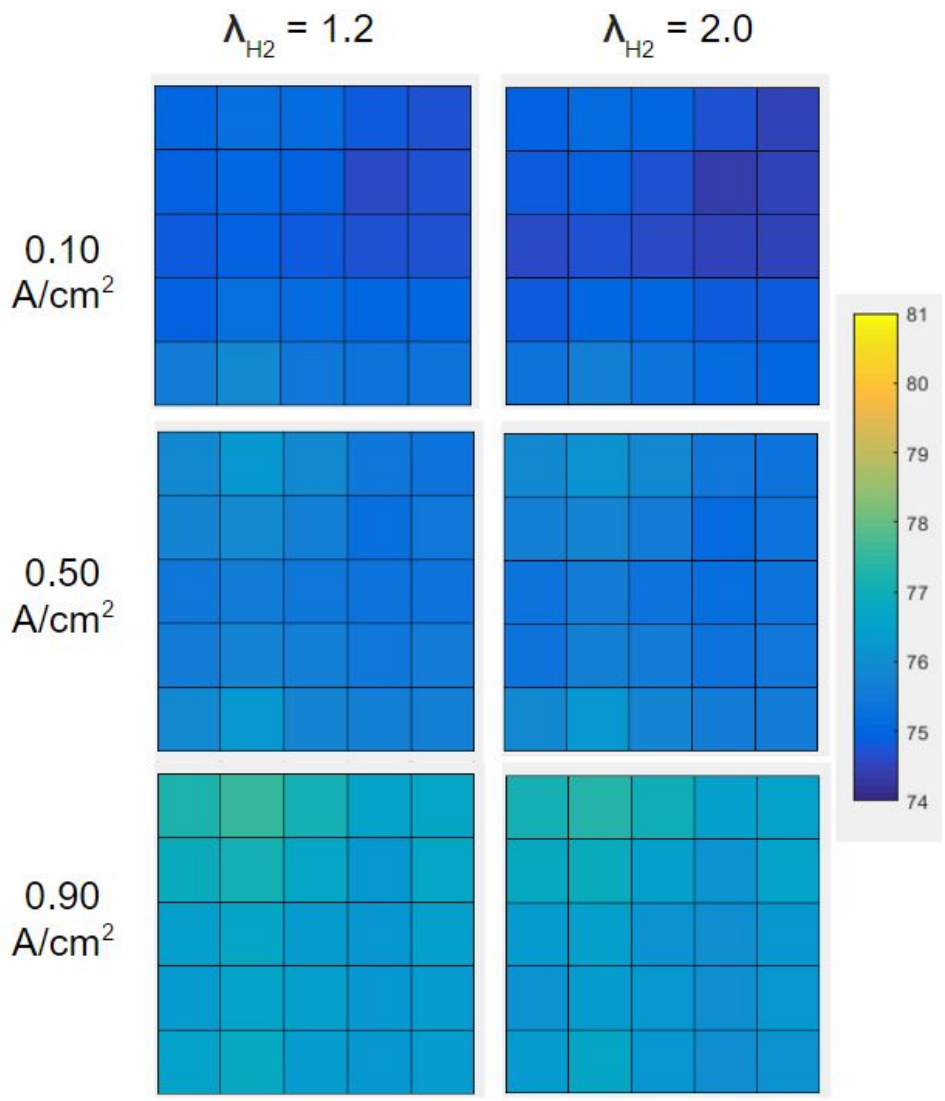

Figure 4-11: 2D pseudocolor maps of temperature distribution at various current density and hydrogen stoichiometric factor settings. Oxygen stoichiometric factor is fixed at 3.0.

H_2 stoichiometry	Maximum temperature (°C)	Minimum temperature (°C)	Average temperature (°C)	Standard deviation from average (°C)
1.2	77.5	74.3	75.7	0.70
2.0	77.4	74.1	75.6	0.70

Table 4-8: Temperature distribution statistics, combining the three different current density settings, at each hydrogen stoichiometric factor setting.

Because temperature varied by less than two degrees within each plot, but varied by seven degrees among all plots, temperature pseudocolor plots were also made with non-standardized scale bars to better understand the temperature distribution within the plate. These plots are shown next to current density distribution data at the same conditions to find any correlations, as shown in **Figure 4-12**. In order to correlate the current and temperature distribution plots more easily, the 12x12 current distribution arrays were reduced to 6x6 arrays by averaging values in 2x2 arrays. These plots are shown in **Figure 4-13**. For each oxygen stoichiometric factor, separated by a vertical black line, the current distribution plots are shown on the left and the temperature distribution plots are shown on the right.

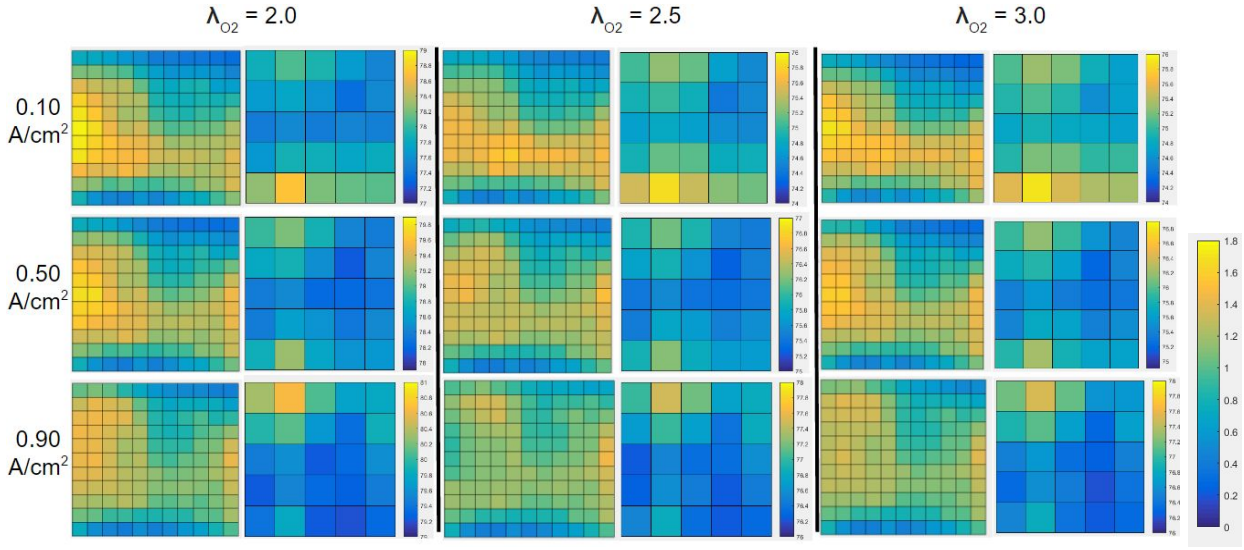

Figure 4-12: 2D pseudocolor maps of current density distribution (12x12 plots) and corresponding temperature distribution at various current density and oxygen stoichiometric factor settings. Hydrogen stoichiometric factor is fixed at 1.2. Scale bar for all the 12x12 current distribution plots is the standardized scale shown on the right. Scale bars for 6x6 temperature plots have a range of 2°C, but different magnitudes.

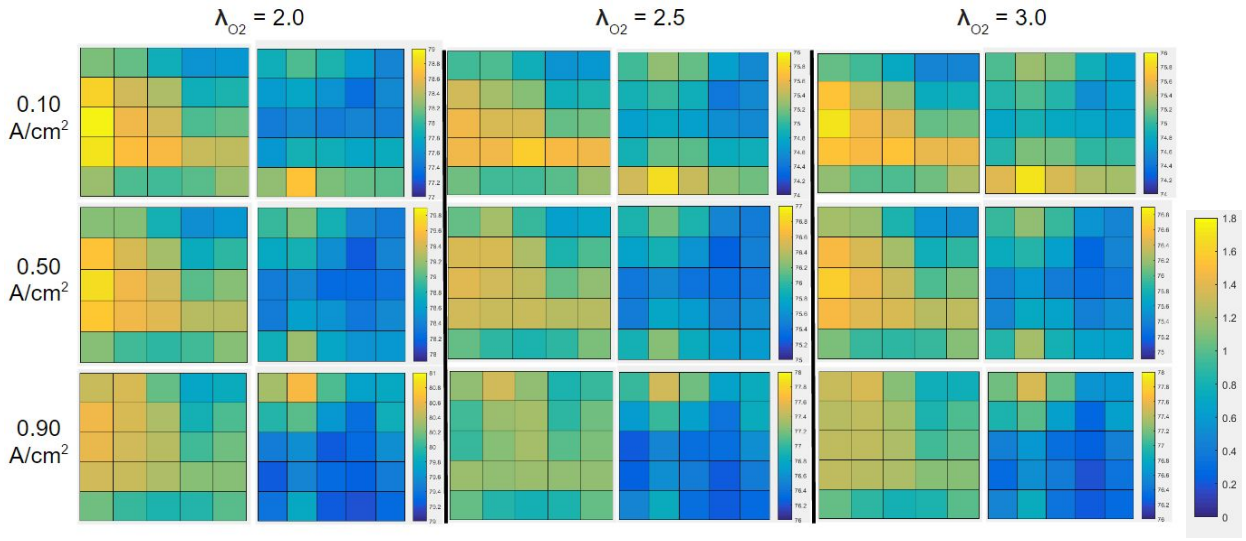

Figure 4-13: 2D pseudocolor maps of current density distribution (6x6 plots) and corresponding temperature distribution at various current density and oxygen stoichiometric factor settings. Hydrogen stoichiometric factor is fixed at 1.2. Scale bar for all the reduced 6x6 current distribution plots is the standardized scale shown on the right. Scale bars for 6x6 temperature plots have a range of 2°C, but different magnitudes.

An interesting result of this comparison is that there is consistently a temperature peak at the bottom left corner of the plate for 0.10 A/cm^2 while there is one at the top left corner for 0.90 A/cm^2. For 0.50 A/cm^2, the temperature peak seems to be distributed between these same top left and bottom left points. This indicates that temperature distribution varies somewhat with current density. The results do not show evidence that temperature distributions vary with the stoichiometric ratios of gases.

Another point of note is that temperature does not vary closely with current density. This may mean that temperature variations are not a direct result of the heat produced by the reaction, but instead a result of the interaction between circulating water (83°C) and fuel gases (~73°C) in a given flow field plate design.

4.5 Comparison of Fresh and Aged Membrane

In order to understand how aging of the membrane affects current distribution, current distribution plots at 0.10, 0.50, and 0.90 A/cm^2 were compared between the fresh and aged form of the same membrane, as shown in **Figure 4-14**.

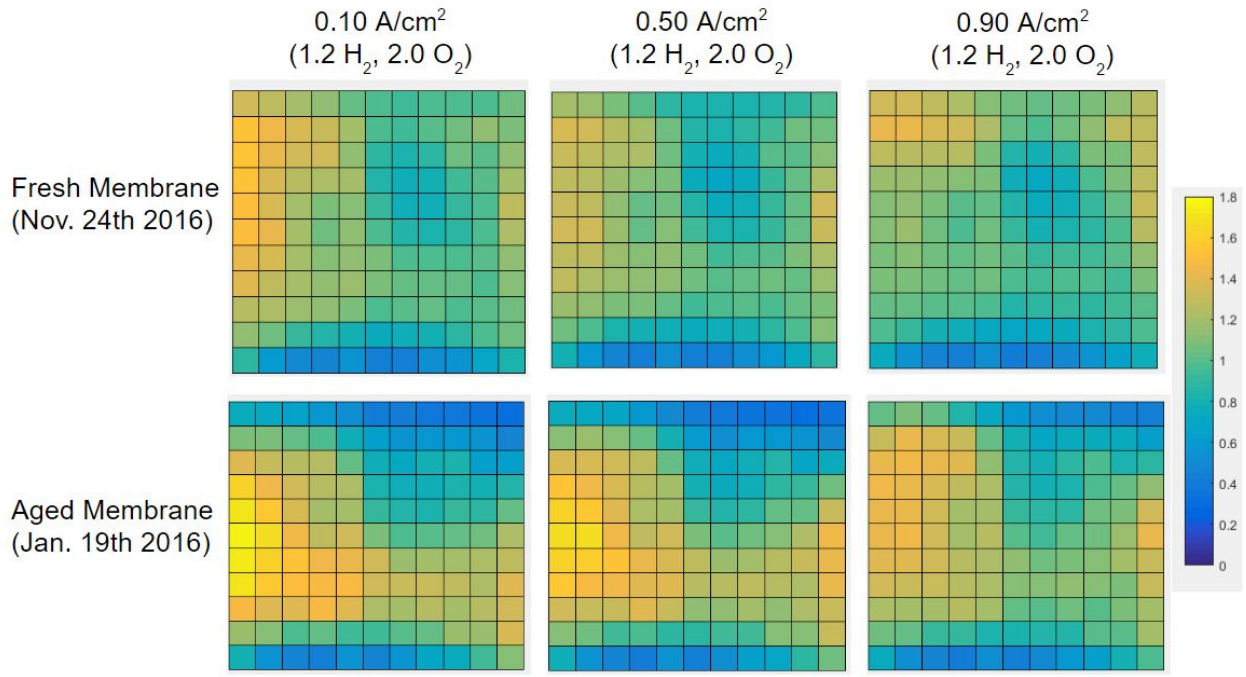

Figure 4-14: Standardized pseudocolor plots of current distribution at 0.10, 0.50, and 0.90 A/cm^2 comparing the same membrane when fresh and when aged.

Comparing the current distributions of the fresh membrane with the aged membrane, it can be seen that the range of current density increases as the membrane ages. This means that the current distribution becomes more uneven as the membrane ages, leading to decreased performance of the fuel cell. A notable trend is that the edges of the plate near the gas inlet and outlet experience a relatively large decrease in current density after aging. This could be due to the high temperatures at the top and bottom edges of the plate (as shown in **Figures 4-12 and 4-13**) that may dry out the membrane faster and lead to accelerated aging of the membrane in these areas. Another interesting point is that areas of the fresh membrane with high current peaks (i.e. the left and right edges of the plate) experience a further increase in current density after aging. This may mean that aging accentuates the uneven current distribution areas in the plate.

Quantitatively, the standard deviation from the average current density doubled from around 0.2 to around 0.4, the minimum values decreased, and the maximum values increased after aging of the membrane, as shown in **Table 4-9**. These statistics further verify that current distribution becomes more uneven after aging of the membrane.

	Current density (A/cm^2)	Maximum standardized value	Minimum standardized value	Average standardized value	Standard deviation from average
Fresh Membrane	**0.10**	1.54	0.43	1.03	0.24
	0.50	1.43	0.51	1.01	0.20
	0.90	1.43	0.41	0.99	0.22
Aged Membrane	**0.10**	1.77	0.16	0.98	0.41
	0.50	1.68	0.15	0.98	0.41
	0.90	1.46	0.20	0.98	0.33

Table 4-9: Statistics of standardized current density data, comparing fresh and aged membrane.

Another method used to compare the fresh and aged membrane was through comparison of the polarization curves, shown in **Figure 4-15**, and comparison of the power curves, shown in **Figure 4-16**. The polarization curve of the fresh membrane is generally above that of the aged membrane, indicating smaller overpotential in the fresh membrane. The power curve shows that the power from the fresh membrane is higher than that of the aged membrane. These results show that the aged membrane has experienced a decrease in performance.

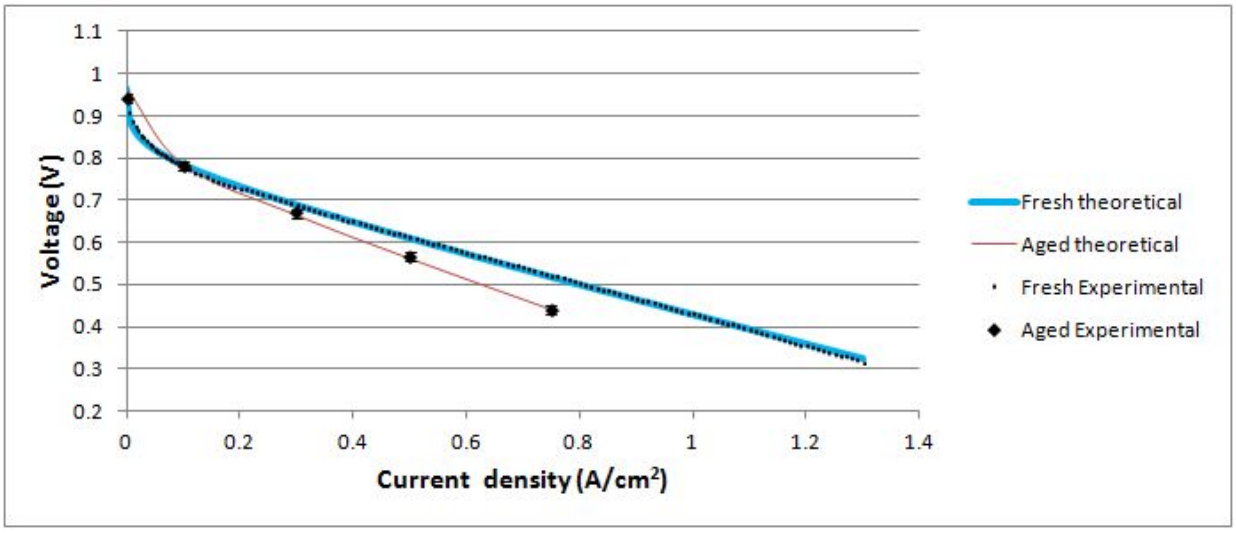

Figure 4-15: Polarization curves of the fresh and aged membrane, showing both experimental and theoretical data.

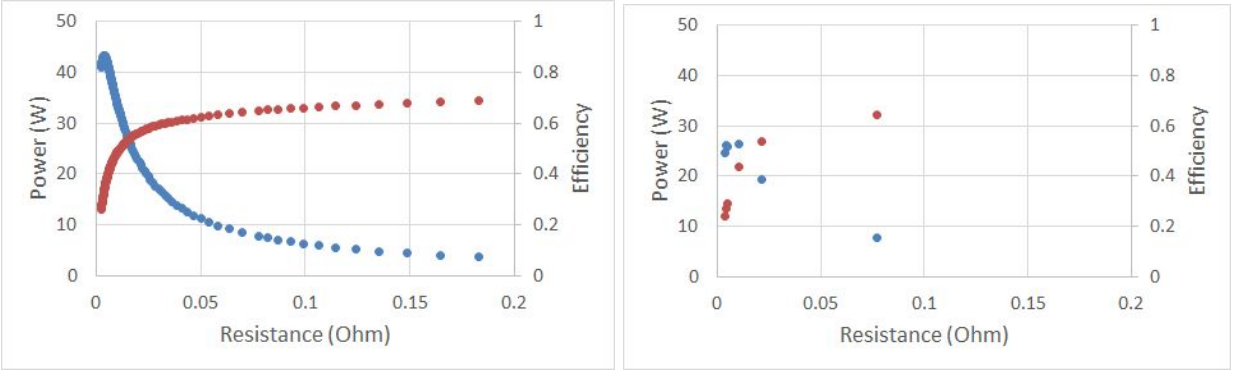

Figure 4-16: Power curves of fresh (left) and aged (right) membrane. Power is plotted in blue and efficiency is plotted in red.

4.6 Comparison of MEA 1 and MEA 2

Current distribution between two MEAs with different gas diffusion layers were compared at 0.10 and 0.50 A/cm^2, shown in **Figure 4-17**. The GDL has a hydrophobic gradient from the inlet to the outlet. MEA 1, the one that was used to compare the current distributions at different current density and gas flow settings, has 18% PTFE in the inlet and the middle and 27% PTFE in the outlet while MEA 2 has 9% PTFE in the inlet and 18% PTFE in the middle and the outlet. Both MEAs were fresh when the current distribution data was collected.

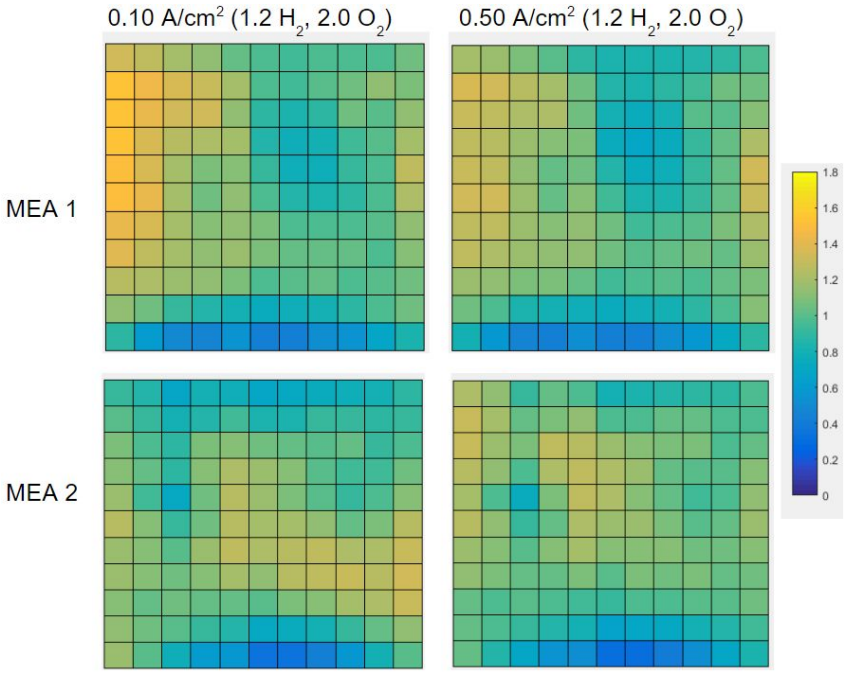

Figure 4-17: Standardized pseudocolor plots at 0.10 and 0.50 A/cm^2 comparing current distributions of MEA 1 and MEA 2.

The two MEAs have different local current density peaks. MEA 1 has peaks concentrated around the left edge of the plate while MEA 2 has peaks concentrated around the center of the plate. Both MEAs have the lowest current density on the bottom edge, near the outlet. These results show that the GDL also affects the current distribution of the fuel cell.

Table 4-10 shows that the standard deviation from the average current density of the MEAs are similar in values, which indicates that the evenness of the current distribution is similar, although the current density is concentrated in different locations. MEA 1, however, has larger maximum and minimum values, which may have a stronger effect on the performance of the fuel cell.

	Current density (A/cm^2)	**Maximum standardized value**	**Minimum standardized value**	**Average standardized value**	**Standard deviation from average**
MEA 1	**0.10**	1.54	0.43	1.03	0.24
	0.50	1.43	0.51	1.01	0.20
MEA 2	**0.10**	1.45	0.34	0.98	0.24
	0.50	1.31	0.31	0.98	0.21

Table 4-10: Statistics of standardized current density data, comparing MEA 1 and MEA 2.

Electrochemical impedance spectroscopy was performed for MEA 2 to observe the performance of the fuel cell because it was suspected that the fuel cell was not performing well due to a faulty membrane. The Nyquist plot for EIS is shown in **Figure 4-18**. EIS was performed at stoichiometric factors of 1.2 for hydrogen and 2.0 for oxygen at current settings of 5, 10, and 15 A. At 20 A and higher, the stoichiometric factors were increased to 1.3 for hydrogen and 2.2 for oxygen to prevent any damage to the fuel cell because the voltage of the system was unstable, which meant that the system may have been experiencing a leak.

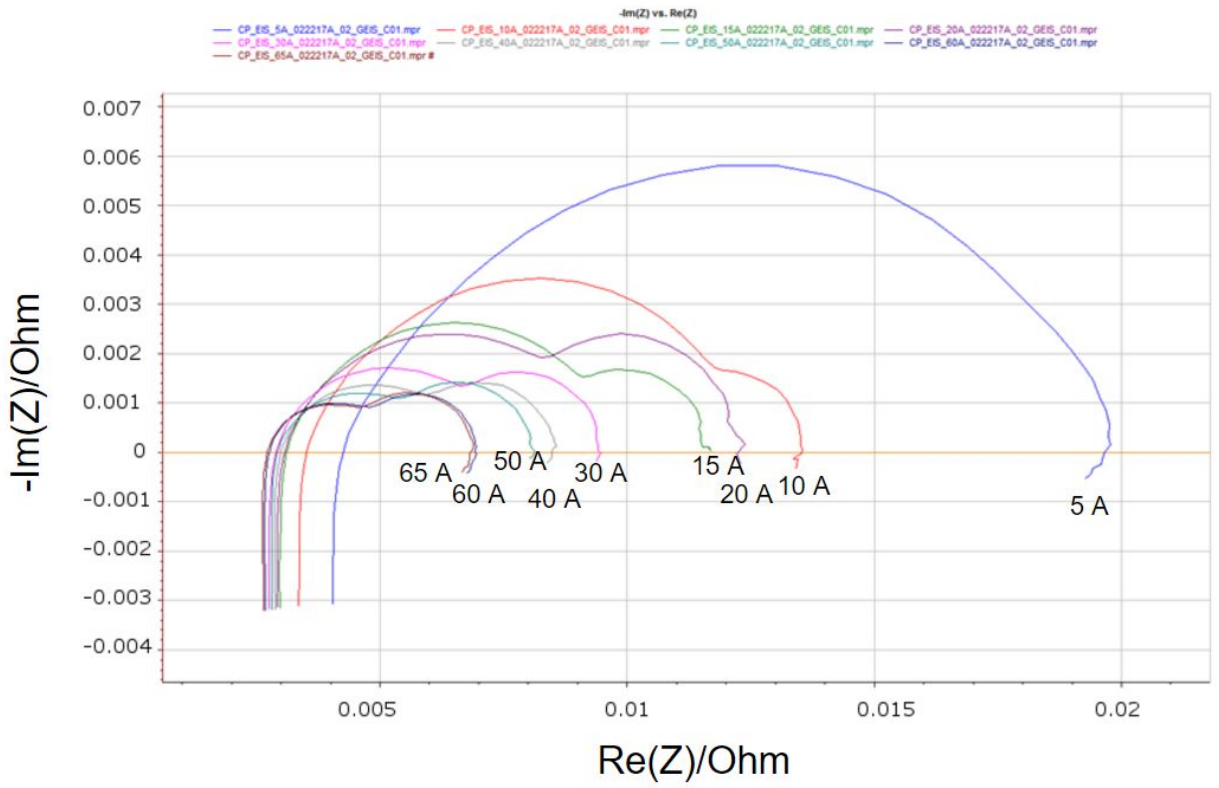

Figure 4-18: Electrochemical impedance spectroscopy results for fresh MEA 2 at current settings of 5, 10, 15, 20, 30, 40, 50, 60, and 65 A.

The EIS results show that increasing the current setting reduces the size of the plot, which means that there is less resistance at higher current settings. Increasing the current setting increases the mass transfer resistance region in relation to the charge transfer resistance region and decreases the ohmic resistance region. The ohmic resistances for each current setting is shown in **Table 4-11**. Comparing the plots for 15 A and 20 A, it can be seen that increasing the stoichiometric factors of the gases increases the mass transfer resistance region.

Current (A)	Ohmic Resistance (Ω)	Stoichiometric Factors
5	$4.27*10^{-3}$	1.2 H_2, 2.0 O_2
10	$3.53*10^{-3}$	1.2 H_2, 2.0 O_2
15	$3.12*10^{-3}$	1.2 H_2, 2.0 O_2
20	$3.08*10^{-3}$	1.3 H_2, 2.2 O_2

30	$2.91*10^{-3}$	1.3 H_2, 2.2 O_2
40	$3.00*10^{-3}$	1.3 H_2, 2.2 O_2
50	$2.94*10^{-3}$	1.3 H_2, 2.2 O_2
60	$2.77*10^{-3}$	1.3 H_2, 2.2 O_2
65	$2.73*10^{-3}$	1.3 H_2, 2.2 O_2

Table 4-11: Ohmic resistance values at each current and stoichiometric factor settings.

Polarization curves (**Figure 4-19**) and power curves (**Figure 4-20**) were constructed as ways to compare the performance of MEA 1 and MEA 2. The polarization curves show that MEA 2 has larger voltage drops than MEA 1 at the same current density, indicating a lower performance for MEA 2. The power curves show that MEA 2 yields less power at the same resistance, which also indicates a lower performance for MEA 2. Because both MEAs are fresh, this means that the different hydrophobic gradients of the MEAs play a role in the degradation of the performance of the fuel cell.

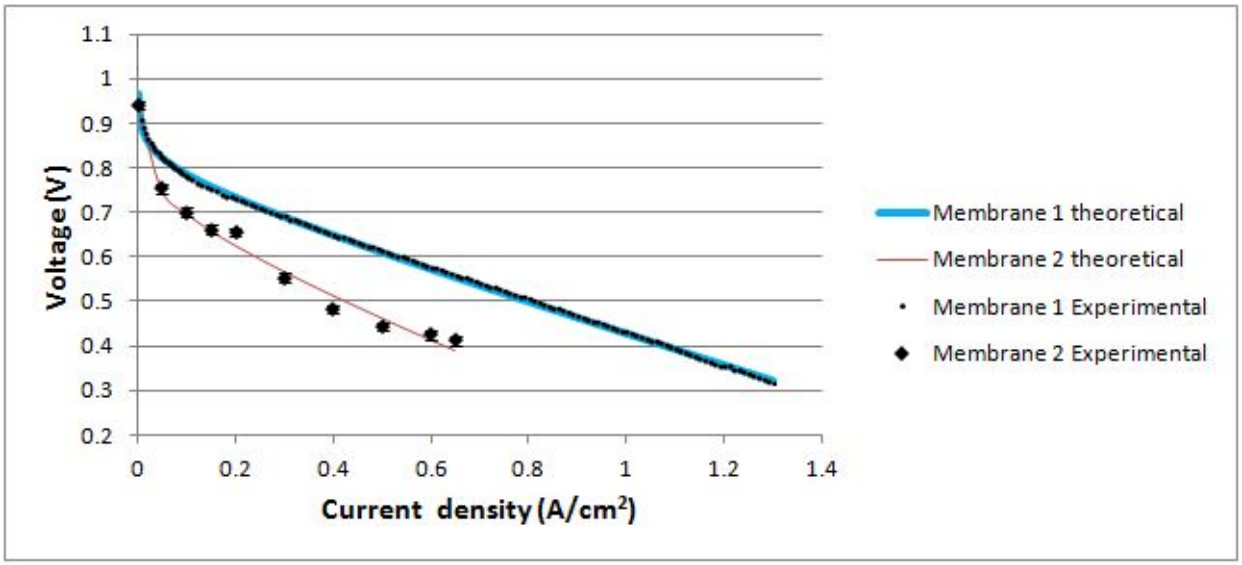

Figure 4-19: Polarization curves of MEA 1 and MEA 2, showing both experimental and theoretical data.

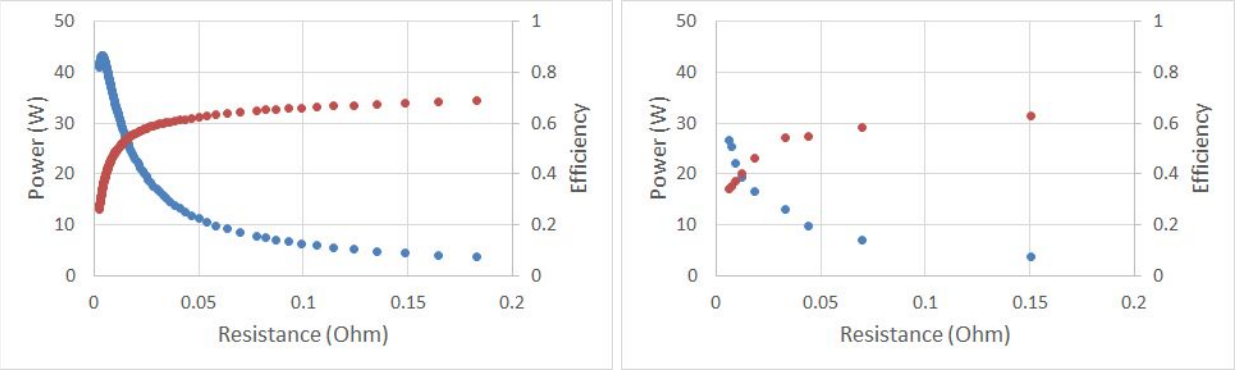

Figure 4-20: Power curves of fresh MEA 1 (left) and fresh MEA 2 (right). Power is plotted in blue and efficiency is plotted in red.

5.0 Conclusion

Because a fuel cell acts as a membrane reactor with plug flow, it was expected that current density would be highest at the inlet where the concentration of reactants is highest and decrease as gases moved towards the outlet. Instead, it was found that the highest current density occurred at the first and fourth bends of the serpentine flow field and that current density was high in the middle of the plate and low at the gas inlet and outlet edges of the plate. Factors that were found to affect the current distribution were as follows: 1) increasing current density decreases the range of current distribution, 2) increasing gas flow slightly increases the evenness of current distribution until a certain point, 3) current density is less evenly distributed after aging of the membrane, and 4) the PTFE composition of the GDL in an MEA affects the location of peaks of current density.

When comparing temperature distribution to the current distribution to see how temperature affects aging of the fuel cell, it was found that there were high temperature peaks at the gas inlet and outlet edges of the plate. These edges were also where there was a large decrease in current density after aging, perhaps indicating that insufficient temperature control in these areas contributed to the accelerated degradation of the membrane.

It would be helpful in the future to recreate these experiments because these results were based on only one trial at each condition due to time restrictions. Additional current density settings, gas flow rates, and pressures would also be interesting to test.

References

Benziger, Jay B., M. Barclay Satterfield, Warren H.J. Hogarth, James P. Nehlsen, and Ioannis G. Kevrekidis. "The Power Performance Curve for Engineering Analysis of Fuel Cells." *Journal of Power Sources* (n.d.): 272-85. *Science Direct*. Science Direct, 27 June 2005. Web. 13 Jan. 2017. <http://pemfc.princeton.edu/Documents/Publications/PowerPerf_2006.pdf>.

Deutschmann, Olaf, and Torsten Kaltschmitt. "Chapter 1: Fuel Processing for Fuel Cells." *Advances in Chemical Engineering: Fuel Cell Engineering*. 1st ed. Vol. 41. Amsterdam: Elsevier, 2012. 1-55. Print.

Hartnig, Christoph, and Christina Roth, eds. *Polymer Electrolyte Membrane and Direct Methanol Fuel Cell Technology*. Vol. 1. New Delhi: Woodhead, 2012. Print.

Hibbert, D. B., and A. M. James. *Dictionary of Electrochemistry*. 2nd ed. London and Basingstoke: Macmillan, 1984. Print.

Lapicque, François, Caroline Bonnet, Bo Tao Huang, and Yohann Chatillon. "Chapter 5: Analysis and Evaluation of Aging Phenomena in PEMFCs." *Advances in Chemical Engineering: Fuel Cell Engineering*. 1st ed. Vol. 41. Amsterdam: Elsevier, 2012. 266-324. 1-118. Print.

Larminie, James, and Andrew Dicks. *Fuel Cell Systems Explained*. 2nd ed. England: Wiley, 2003. Print.

Lobato, Justo, et al. "Study of flow channel geometry using current distribution measurement in a high temperature polymer electrolyte membrane fuel cell." *Journal of Power Sources* 196.9 (2011): 4209-4217.

Thampan, Tony, et al. "PEM fuel cell as a membrane reactor." *Catalysis Today* 67.1 (2001): 15-32.

Úbeda, Diego, et al. "Durability study of HTPEMFC through current distribution measurements and the application of a model." *International Journal of Hydrogen Energy* 39.36 (2014): 21678-21687.

Wagner, N., et al. "Electrochemical impedance spectra of solid-oxide fuel cells and polymer membrane fuel cells." *Electrochimica Acta* 43.24 (1998): 3785-3793.

Wang, Haijiang, Xiao-Zi Yuan, and Hui Li, eds. *PEM fuel cell diagnostic tools*. Vol. 2. CRC press, 2011.

Weber, Adam Z., Sivagaminathan Balasubramanian, and Prodip K. Das. "Chapter 2: Proton Exchange Membrane Fuel Cells." *Advances in Chemical Engineering: Fuel Cell Engineering*. 1st ed. Vol. 41. Amsterdam: Elsevier, 2012. 65-139. Print.

Appendices

Appendix A: Standardized Current Density Averages

Table A-1: Current density averages at 1.5 bar, λ_{H2} =1.2, λ_{O2} =2.0, 0.10 A/cm^2

					MAX	MIN	AVG	STDEV			
AVERAGE STANDARDIZED CD					1.767168	0.159048	0.980244	0.412292			
0.448344	0.372096	0.338112	0.286848	0.281736	0.207432	0.20412	0.187704	0.159048	0.17604	0.219744	0.219888
0.739008	0.708048	0.671904	0.57168	0.510408	0.415656	0.405216	0.384264	0.367776	0.338112	0.33624	0.28332
1.094184	1.083168	1.022544	0.98388	0.780624	0.622872	0.542736	0.588672	0.567216	0.537048	0.455112	0.381456
1.398888	1.32156	1.262304	1.24596	1.035432	0.783	0.72828	0.793656	0.820224	0.639144	0.646128	0.592128
1.627272	1.445904	1.3338	1.2492	1.215936	0.827856	0.77256	0.781488	0.827784	0.797832	0.860616	0.857304
1.700352	1.553544	1.371744	1.208664	1.200888	0.917352	0.854208	0.833472	0.92304	0.88092	1.039536	1.068192
1.767168	1.66032	1.443744	1.290096	1.3482	1.086984	0.976104	1.009008	1.01412	1.068408	1.212192	1.214064
1.73556	1.613808	1.52064	1.436184	1.423584	1.329696	1.181016	1.184544	1.19268	1.237464	1.2906	1.32732
1.689624	1.548864	1.497168	1.464912	1.470312	1.33884	1.308024	1.319472	1.283112	1.222344	1.402056	1.402776
1.466496	1.388448	1.379088	1.469736	1.397808	1.216368	1.197144	1.24488	1.188144	1.259568	1.337472	1.385784
1.171368	1.114632	0.975672	1.015488	0.94392	0.953568	1.007496	1.022328	1.173888	1.161	1.375776	1.362384
0.799344	0.554184	0.470448	0.428184	0.560952	0.46728	0.546552	0.691344	0.752256	0.943128	1.117656	1.19592

Table A-2: Current density averages at 1.5 bar, λ_{H2} =1.2, λ_{O2} =2.0, 0.50 A/cm^2

					MAX	MIN	AVG	STDEV			
AVERAGE STANDARDIZED CD					1.676635	0.149242	0.980474	0.406468			
0.431309	0.364032	0.336341	0.282672	0.274104	0.198547	0.190109	0.174154	0.149242	0.167026	0.215568	0.22284
0.73129	0.730771	0.700906	0.581832	0.503597	0.39865	0.381038	0.362707	0.354398	0.330768	0.339696	0.296726
1.108066	1.158725	1.098389	1.038125	0.79164	0.606888	0.524088	0.575539	0.568627	0.552614	0.482717	0.425765
1.372133	1.373602	1.325981	1.280016	1.030046	0.762422	0.707789	0.786024	0.84744	0.694627	0.735278	0.715522
1.545134	1.458749	1.362658	1.262218	1.204142	0.804514	0.756432	0.78673	0.8838	0.914112	1.049918	1.086293
1.612642	1.558195	1.397419	1.217102	1.19232	0.907877	0.859219	0.878054	1.02515	1.034395	1.307333	1.368634
1.676635	1.662091	1.459051	1.292155	1.33439	1.069877	0.989755	1.056917	1.113955	1.215158	1.455653	1.468555
1.627142	1.602086	1.526803	1.406837	1.369152	1.276128	1.156162	1.191442	1.239149	1.320019	1.413317	1.451664
1.554941	1.487045	1.454429	1.399018	1.386778	1.260302	1.246075	1.271779	1.264277	1.224518	1.415088	1.389413
1.342325	1.3104	1.317816	1.39379	1.314835	1.147104	1.1268	1.185048	1.141474	1.228277	1.311898	1.325434
1.097986	1.063325	0.93685	0.969365	0.890539	0.890957	0.940219	0.949363	1.099051	1.102061	1.309738	1.266509
0.772186	0.540317	0.463709	0.421646	0.541339	0.445349	0.50881	0.632131	0.688493	0.877046	1.051934	1.102925

Table A-3: Current density averages at 1.5 bar, λ_{H2} =1.2, λ_{O2} =2.0, 0.90 A/cm^2

					MAX	MIN	AVG	STDEV			
AVERAGE STANDARDIZED CD					1.582848	0.196632	0.981312	0.385619			
0.456264	0.403488	0.397656	0.357984	0.367776	0.260424	0.252216	0.227088	0.196632	0.216648	0.26748	0.274896
0.704016	0.710064	0.72576	0.64152	0.595296	0.479088	0.46476	0.444816	0.425088	0.39492	0.400032	0.349416
0.948384	0.979776	0.98064	0.955944	0.77868	0.63324	0.556128	0.606744	0.581544	0.582192	0.531576	0.466128
1.151064	1.14408	1.127376	1.124928	0.945288	0.732384	0.675504	0.73728	0.773928	0.67428	0.716112	0.688464
1.34964	1.266768	1.209312	1.148616	1.11924	0.795528	0.762264	0.76572	0.828144	0.814104	0.939528	0.985032
1.42308	1.38456	1.263024	1.140696	1.170576	0.913176	0.872928	0.850536	0.947304	0.913824	1.158984	1.2474
1.455192	1.458216	1.355184	1.272168	1.353456	1.126152	1.020672	1.05444	1.054368	1.128456	1.363608	1.404504
1.43568	1.416168	1.44396	1.473696	1.510128	1.448136	1.305648	1.315296	1.323144	1.346904	1.410264	1.463184
1.43604	1.386936	1.442304	1.525248	1.582848	1.475496	1.476144	1.47852	1.437192	1.339128	1.487592	1.486296
1.281816	1.258488	1.314792	1.47312	1.43316	1.298808	1.314864	1.36584	1.294056	1.353312	1.39176	1.428696
1.068408	1.023336	0.936576	0.979416	0.932256	0.935208	0.989568	0.984456	1.156968	1.176696	1.367208	1.369512
0.781632	0.532152	0.438984	0.431928	0.574848	0.476136	0.536112	0.648	0.716904	0.898272	1.089648	1.188576

Table A-4: Current density averages at 1.5 bar, λ_{H2} =1.2, λ_{O2} =2.5, 0.10 A/cm^2

					MAX	MIN	AVG	STDEV			
AVERAGE STANDARDIZED CD					1.459536	0.200648	0.980356	0.333817			
0.665272	0.5784	0.528936	0.431512	0.400288	0.28052	0.263456	0.238216	0.200648	0.220712	0.276192	0.27532
1.037192	1.075696	1.025864	0.86792	0.727976	0.566584	0.52772	0.496648	0.484584	0.44848	0.443744	0.36684
1.32044	1.41592	1.371352	1.302352	1.024656	0.791264	0.680112	0.740456	0.741568	0.737456	0.621352	0.50656
1.41224	1.441288	1.430472	1.397536	1.135272	0.856552	0.807528	0.897536	0.980624	0.838496	0.875528	0.798592
1.436744	1.41272	1.367128	1.283656	1.229856	0.85148	0.807752	0.842888	0.958488	1.01568	1.148344	1.157648
1.428376	1.421216	1.33264	1.19344	1.182608	0.908008	0.880272	0.899048	1.0502	1.070584	1.338824	1.3926
1.434096	1.459536	1.324584	1.20204	1.248576	1.009184	0.949072	1.013888	1.060896	1.15748	1.413664	1.42672
1.381744	1.383152	1.343656	1.248328	1.228208	1.152144	1.04908	1.083632	1.124312	1.208264	1.320048	1.36516
1.347472	1.30512	1.294568	1.2472	1.234968	1.12068	1.109056	1.12924	1.120976	1.093656	1.295	1.285352
1.217208	1.200856	1.206816	1.262048	1.188496	1.033256	1.002664	1.046952	1.010736	1.095264	1.188464	1.213992
1.047296	1.018584	0.90116	0.913712	0.827576	0.82248	0.859848	0.86588	0.99404	0.991424	1.18924	1.156584
0.757296	0.528904	0.456968	0.417752	0.527776	0.429224	0.478552	0.588328	0.630344	0.803256	0.961248	1.0022

Table A-5: Current density averages at 1.5 bar, λ_{H2} =1.2, λ_{O2} =2.5, 0.50 A/cm^2

					MAX	MIN	AVG	STDEV			
AVERAGE STANDARDIZED CD					1.513282	0.205186	0.98062	0.344999			
0.478152	0.436349	0.43691	0.386597	0.392227	0.275256	0.263232	0.236088	0.205186	0.228139	0.285854	0.294581
0.752573	0.807955	0.85788	0.750557	0.676238	0.535291	0.510782	0.48888	0.474754	0.438811	0.442224	0.3798
1.020542	1.150445	1.194696	1.165003	0.926496	0.727603	0.629842	0.687542	0.675058	0.684	0.61164	0.523598
1.201838	1.281312	1.32336	1.31243	1.075406	0.818626	0.759125	0.837461	0.909605	0.813946	0.855432	0.80208
1.367179	1.371182	1.352664	1.273507	1.21729	0.865886	0.830549	0.85644	0.972432	0.987264	1.139472	1.163722
1.410264	1.439107	1.353773	1.208203	1.212307	0.942912	0.929851	0.942955	1.093435	1.083038	1.381594	1.446926
1.389413	1.440979	1.334995	1.232798	1.289203	1.075853	1.017317	1.086667	1.137787	1.227802	1.50768	1.513282
1.310198	1.309262	1.277438	1.247328	1.289318	1.261066	1.172693	1.214222	1.258373	1.320422	1.397678	1.423526
1.345363	1.308082	1.29875	1.293538	1.309925	1.224058	1.238357	1.257077	1.247789	1.208261	1.364674	1.323965
1.237709	1.208189	1.218874	1.294229	1.231085	1.109102	1.120781	1.176782	1.135728	1.221538	1.283659	1.262189
1.034078	0.981086	0.88321	0.896371	0.833285	0.831787	0.880056	0.898142	1.06979	1.099022	1.277165	1.218154
0.759773	0.511646	0.419688	0.406843	0.529661	0.439517	0.498571	0.608861	0.674712	0.853243	1.021997	1.064203

Table A-6: Current density averages at 1.5 bar, λ_{H_2} =1.2, λ_{O_2} =2.5, 0.90 A/cm^2

					MAX	MIN	AVG	STDEV			
AVERAGE STANDARDIZED CD					1.4778	0.30628	0.980346	0.263092			
0.656056	0.562392	0.578808	0.511216	0.528696	0.380312	0.372168	0.345032	0.30628	0.341304	0.441376	0.447728
0.960664	1.034584	1.098336	1.010264	0.92028	0.767072	0.730912	0.705672	0.696624	0.6584	0.699896	0.585096
1.136368	1.28152	1.3404	1.327488	1.131888	0.941808	0.836024	0.91964	0.926304	0.963872	0.897216	0.751704
1.05044	1.175064	1.275864	1.321928	1.135392	0.924064	0.891	0.995216	1.083496	0.99464	1.093864	0.999728
0.92992	1.086992	1.181072	1.194704	1.200384	0.90972	0.88436	0.9168	1.04312	1.093344	1.262456	1.277432
0.887168	1.055592	1.12276	1.108376	1.171704	0.943248	0.947752	0.950104	1.092456	1.090912	1.396536	1.46724
0.911616	1.065328	1.099792	1.104968	1.203536	1.0284	0.988872	1.045736	1.080224	1.16476	1.459024	1.4778
0.98084	1.044592	1.097312	1.117784	1.173344	1.15972	1.095088	1.134016	1.16688	1.231864	1.342776	1.392488
1.158384	1.134064	1.149208	1.15908	1.180656	1.109464	1.133744	1.154472	1.148208	1.124128	1.320088	1.312024
1.165112	1.127288	1.125616	1.187304	1.131608	1.01804	1.032464	1.08872	1.056152	1.142888	1.232416	1.242168
1.0372	0.969184	0.861536	0.8598	0.788072	0.78916	0.818656	0.837648	1.012904	1.031976	1.22384	1.180008
0.777592	0.514008	0.424632	0.413272	0.526976	0.431672	0.482448	0.58836	0.64484	0.813552	0.976248	1.01796

Table A-7: Current density averages at 1.5 bar, λ_{H_2} =1.2, λ_{O_2} =3.0, 0.10 A/cm^2

					MAX	MIN	AVG	STDEV			
AVERAGE STANDARDIZED CD					1.694808	0.148968	0.981232	0.426536			
0.458712	0.396144	0.357552	0.306576	0.301032	0.208512	0.196992	0.174168	0.148968	0.163944	0.199944	0.213264
0.735912	0.699624	0.665856	0.56088	0.489816	0.393984	0.369864	0.341712	0.313488	0.277848	0.287712	0.266544
1.040112	1.01304	0.9486	0.894168	0.709776	0.562248	0.476496	0.499752	0.453312	0.41904	0.384264	0.363384
1.307088	1.239768	1.170288	1.140696	0.946872	0.727488	0.657288	0.687024	0.684792	0.544104	0.56664	0.5706
1.525176	1.382616	1.283616	1.196136	1.14984	0.803808	0.74916	0.73728	0.769536	0.70884	0.80424	0.856152
1.62504	1.521432	1.34424	1.185264	1.196784	0.91476	0.865872	0.831312	0.912816	0.855864	1.069056	1.145592
1.694808	1.632024	1.446696	1.313496	1.381176	1.139544	1.024992	1.059192	1.05984	1.122264	1.327968	1.355184
1.615536	1.571328	1.529136	1.496808	1.518336	1.454256	1.306584	1.32408	1.327464	1.354752	1.416528	1.463256
1.534464	1.46664	1.473552	1.49328	1.542384	1.43388	1.41264	1.441296	1.409832	1.327176	1.509768	1.507104
1.333728	1.29672	1.327968	1.446624	1.3932	1.249056	1.257768	1.315656	1.2762	1.353384	1.430136	1.464768
1.138968	1.098144	1.008576	1.039536	0.982008	0.990792	1.045512	1.047384	1.225728	1.213632	1.429344	1.415952
0.855504	0.606456	0.502488	0.497088	0.641088	0.530352	0.590976	0.707256	0.773928	0.964008	1.158336	1.23156

Table A-8: Current density averages at 1.5 bar, λ_{H_2} =1.2, λ_{O_2} =3.0, 0.50 A/cm^2

					MAX	MIN	AVG	STDEV			
AVERAGE STANDARDIZED CD					1.596845	0.156298	0.980288	0.390661			
0.52069	0.453154	0.411178	0.337997	0.324518	0.219053	0.204984	0.182218	0.156298	0.17447	0.217022	0.22919
0.86089	0.867643	0.82368	0.673963	0.566366	0.443995	0.409608	0.380981	0.356198	0.317434	0.325397	0.293126
1.203811	1.247818	1.173053	1.09129	0.839506	0.640958	0.53712	0.570355	0.534326	0.504259	0.453758	0.414418
1.380082	1.384315	1.342267	1.295093	1.044691	0.786413	0.711216	0.763805	0.802411	0.664718	0.69084	0.68197
1.486037	1.442995	1.373371	1.272557	1.199405	0.832406	0.781286	0.789206	0.873677	0.850925	0.990058	1.048478
1.545624	1.522627	1.369138	1.197605	1.191614	0.899554	0.86881	0.86413	0.994421	0.977342	1.272499	1.366402
1.596845	1.595174	1.417046	1.266696	1.303085	1.059826	0.972648	1.029154	1.069618	1.159747	1.445933	1.490587
1.537474	1.53301	1.467792	1.385078	1.36885	1.290989	1.169179	1.20695	1.245874	1.306354	1.411992	1.471838
1.464322	1.412971	1.395792	1.370304	1.371197	1.253102	1.237882	1.268597	1.268323	1.224691	1.433578	1.429978
1.272067	1.23781	1.241251	1.315872	1.247962	1.10772	1.103918	1.166746	1.148098	1.242014	1.347365	1.38803
1.0764	1.02852	0.927202	0.942581	0.876686	0.876456	0.92687	0.939701	1.113768	1.12271	1.355962	1.340611
0.797789	0.556992	0.462888	0.451987	0.575539	0.473789	0.530294	0.643147	0.70992	0.901008	1.096286	1.164326

Table A-9: Current density averages at 1.5 bar, λ_{H_2} =1.2, λ_{O_2} =3.0, 0.90 A/cm^2

					MAX	MIN	AVG	STDEV			
AVERAGE STANDARDIZED CD					1.416744	0.242448	0.980532	0.296519			
0.69572	0.615048	0.588232	0.504528	0.49956	0.340584	0.31852	0.284408	0.242448	0.268	0.337792	0.348368
1.078264	1.11816	1.12644	1.005704	0.879136	0.709368	0.645216	0.595416	0.558328	0.50488	0.514352	0.439744
1.316232	1.378144	1.369136	1.324984	1.106264	0.88364	0.760496	0.804568	0.784296	0.782624	0.702136	0.5946
1.306968	1.323096	1.344376	1.344896	1.126888	0.896456	0.84352	0.920256	0.993504	0.881064	0.943384	0.867008
1.263776	1.282704	1.286976	1.243936	1.206952	0.880336	0.842304	0.8626	0.97592	0.999104	1.149856	1.170904
1.258032	1.310576	1.26264	1.163304	1.181384	0.911112	0.898272	0.895336	1.031248	1.023296	1.316472	1.386336
1.285008	1.355944	1.269728	1.180736	1.230976	1.007688	0.9354	0.987016	1.015264	1.101648	1.392632	1.416744
1.26192	1.297968	1.279816	1.225064	1.224856	1.16668	1.066608	1.100088	1.127648	1.187176	1.295808	1.354096
1.276176	1.247776	1.244368	1.225104	1.224688	1.117608	1.103848	1.124608	1.120376	1.086864	1.289184	1.289528
1.179976	1.153456	1.14792	1.207776	1.142072	0.99648	0.982168	1.034768	1.012704	1.097144	1.200576	1.22876
1.030592	0.9848	0.884288	0.881552	0.802992	0.791512	0.822672	0.838016	0.992776	0.99992	1.20696	1.178744
0.789872	0.5346	0.444128	0.429256	0.535752	0.43324	0.479536	0.577336	0.632976	0.804312	0.975192	1.025056

Table A-10: Current density averages at 1.5 bar, λ_{H_2} =2.0, λ_{O_2} =3.0, 0.10 A/cm^2

					MAX	MIN	AVG	STDEV			
AVERAGE STANDARDIZED CD					1.657728	0.227376	0.981628	0.361974			
0.581256	0.497808	0.476424	0.42228	0.430848	0.307944	0.2934	0.26244	0.227376	0.24624	0.302832	0.30744
0.875592	0.85572	0.846504	0.742896	0.670032	0.538488	0.50976	0.480672	0.45936	0.42408	0.44208	0.383688
1.15992	1.148616	1.09728	1.05336	0.851256	0.685152	0.592056	0.638136	0.61632	0.605808	0.555912	0.494352
1.366056	1.300752	1.234656	1.20492	0.9954	0.768096	0.719352	0.775368	0.801864	0.678672	0.736272	0.714096
1.544688	1.406736	1.300824	1.208664	1.167912	0.811872	0.758016	0.761184	0.831096	0.850896	0.967032	0.998424
1.614024	1.516824	1.344816	1.180008	1.188792	0.92376	0.876456	0.859824	0.958968	0.921744	1.15776	1.233072
1.657728	1.599552	1.419048	1.283688	1.334952	1.0998	1.005336	1.035144	1.038528	1.100088	1.308168	1.33668
1.598472	1.528992	1.479672	1.426032	1.435392	1.360368	1.216872	1.221336	1.227096	1.254744	1.301616	1.35432
1.512864	1.423152	1.413072	1.422216	1.45692	1.327536	1.284984	1.313712	1.289736	1.22184	1.347768	1.337328
1.27368	1.22904	1.257768	1.367352	1.298088	1.134072	1.121976	1.183968	1.136736	1.211904	1.26288	1.269936
1.04436	0.997272	0.908568	0.93528	0.878832	0.889056	0.920736	0.914184	1.085616	1.05876	1.238544	1.20888
0.75996	0.520848	0.429408	0.418464	0.55224	0.457056	0.511344	0.614592	0.666144	0.819648	0.9828	1.057464

Table A-11: Current density averages at 1.5 bar, λ_{H_2} =2.0, λ_{O_2} =3.0, 0.50 A/cm^2

					MAX	MIN	AVG	STDEV			
AVERAGE STANDARDIZED CD					1.498464	0.268157	0.98041	0.315074			
0.785434	0.673272	0.635976	0.542909	0.530482	0.367776	0.346723	0.310147	0.268157	0.29389	0.368424	0.376862
1.168502	1.158062	1.127376	0.978494	0.858326	0.677549	0.631224	0.591638	0.57312	0.535277	0.554875	0.473126
1.422518	1.43388	1.389082	1.323965	1.062691	0.843552	0.719957	0.780336	0.769666	0.780293	0.71316	0.610402
1.446163	1.430525	1.416989	1.392912	1.136866	0.872222	0.81576	0.891605	0.957082	0.839174	0.908107	0.841723
1.438747	1.433894	1.397952	1.306656	1.239336	0.868162	0.81864	0.832838	0.936806	0.984298	1.111306	1.126094
1.456589	1.472386	1.364645	1.205741	1.200341	0.922954	0.891202	0.884736	1.011442	0.999418	1.25771	1.329509
1.463803	1.498464	1.363277	1.230826	1.255666	1.02227	0.945014	0.984571	1.005192	1.08517	1.337587	1.367338
1.39343	1.395389	1.356034	1.28065	1.271635	1.188418	1.068869	1.088496	1.115208	1.166342	1.250107	1.310429
1.305936	1.257106	1.249675	1.219882	1.230854	1.105214	1.087646	1.114373	1.109477	1.078099	1.246925	1.25843
1.118952	1.091966	1.100448	1.168978	1.102392	0.954086	0.937094	0.99167	0.970042	1.065514	1.151885	1.183075
0.922522	0.884952	0.797227	0.806803	0.749146	0.752098	0.777758	0.783994	0.93659	0.937858	1.137773	1.117642
0.677146	0.46489	0.37993	0.367618	0.475445	0.391262	0.436608	0.532195	0.58703	0.739598	0.899078	0.96228

Table A-12: Current density averages at 1.5 bar, λ_{H_2} =2.0, λ_{O_2} =3.0, 0.90 A/cm^2

					MAX	MIN	AVG	STDEV			
AVERAGE STANDARDIZED CD					1.467216	0.358048	0.980526	0.272523			
0.900424	0.79304	0.754288	0.664656	0.658752	0.472888	0.451896	0.411376	0.358048	0.387408	0.487704	0.496712
1.248816	1.263416	1.261344	1.140024	1.021408	0.835544	0.785872	0.745944	0.732008	0.691656	0.72824	0.618352
1.430736	1.467216	1.452768	1.399976	1.162328	0.948104	0.83024	0.907976	0.916464	0.9512	0.887536	0.759328
1.404416	1.398904	1.404192	1.38884	1.144784	0.902824	0.864336	0.956888	1.03192	0.930056	1.047624	0.971504
1.372224	1.365024	1.336632	1.2588	1.203088	0.860496	0.815168	0.83872	0.957592	1.03324	1.182064	1.201376
1.364704	1.373664	1.282928	1.14328	1.139688	0.8824	0.859792	0.860688	0.991672	0.994128	1.270416	1.346296
1.364552	1.391824	1.2642	1.145464	1.169224	0.950472	0.887384	0.926688	0.953032	1.038432	1.30324	1.333976
1.295968	1.29892	1.24912	1.168576	1.158928	1.083616	0.977448	0.9962	1.021424	1.090112	1.194272	1.258064
1.239248	1.194016	1.16588	1.121392	1.125792	1.004176	0.978424	1.002568	0.99828	0.990888	1.177936	1.188464
1.09988	1.074208	1.068096	1.113816	1.037408	0.879832	0.848464	0.89624	0.877072	0.97796	1.080552	1.113432
0.949752	0.913136	0.811424	0.799936	0.722784	0.715896	0.727592	0.732696	0.878368	0.872656	1.072256	1.050984
0.707184	0.484376	0.395912	0.3786	0.47596	0.383568	0.42256	0.510608	0.555936	0.701336	0.85056	0.902488

Appendix B: Temperature Averages

Table B-1: Temperature averages at 1.5 bar, λ_{H2} =1.2, λ_{O2} =2.0, 0.10 A/cm^2

78.05849	77.99096	77.89591	77.72847	77.86873	77.72312
77.85368	78.08067	77.92147	77.66516	77.52878	77.53507
77.67467	77.77315	77.61842	77.3657	77.53572	77.1488
77.44926	77.53538	77.44837	77.52736	77.49977	77.09402
77.6533	77.88531	77.85216	77.77333	77.82443	77.66196
78.25582	78.7043	78.20484	78.1263	78.09478	78.03702

Table B-2: Temperature averages at 1.5 bar, λ_{H2} =1.2, λ_{O2} =2.0, 0.50 A/cm^2

78.9239	78.82323	78.65094	78.33919	78.53283	78.40311
78.90739	79.11813	78.80535	78.42108	78.34993	78.30089
78.711	78.78605	78.46557	78.12386	78.40374	78.01258
78.34324	78.44998	78.22576	78.22875	78.30167	77.91761
78.35399	78.60887	78.50257	78.33596	78.46115	78.32539
78.76129	79.19332	78.65738	78.52402	78.54819	78.54669

Table B-3: Temperature averages at 1.5 bar, λ_{H2} =1.2, λ_{O2} =2.0, 0.90 A/cm^2

80.22232	80.08515	79.74714	79.45075	79.71466	79.583
80.33508	80.62617	80.09063	79.72789	79.78848	79.66467
79.96526	80.11112	79.62854	79.36532	79.86195	79.52917
79.44342	79.58968	79.2469	79.34196	79.58826	79.32158
79.23223	79.5068	79.33239	79.25261	79.46256	79.41994
79.40284	79.80158	79.23043	79.19655	79.31969	79.41319

Table B-4: Temperature averages at 1.5 bar, λ_{H2} =1.2, λ_{O2} =2.5, 0.10 A/cm^2

75.23484	75.20831	75.16554	74.74563	74.77956	74.69581
75.03796	75.27854	75.15081	74.70558	74.56158	74.53706
74.88319	75.02298	74.86866	74.41882	74.55335	74.17361
74.6936	74.79774	74.71812	74.59231	74.55285	74.13576
74.88029	75.13418	75.10192	74.83805	74.87036	74.68407
75.46897	75.85943	75.45672	75.2212	75.16348	75.06303

Table B-5: Temperature averages at 1.5 bar, λ_{H_2} =1.2, λ_{O_2} =2.5, 0.50 A/cm^2

75.93983	75.92998	75.82513	75.4374	75.52314	75.44837
75.90891	76.18014	75.93454	75.52371	75.44949	75.39406
75.74657	75.88775	75.622	75.25459	75.49993	75.10985
75.40697	75.5436	75.39016	75.36561	75.42579	75.02966
75.46638	75.75679	75.66195	75.47516	75.56266	75.39595
75.8792	76.24685	75.81636	75.6839	75.68204	75.63049

Table B-6: Temperature averages at 1.5 bar, λ_{H_2} =1.2, λ_{O_2} =2.5, 0.90 A/cm^2

76.91142	76.96827	76.85211	76.46731	76.67073	76.60926
77.00637	77.47893	77.18219	76.74383	76.8237	76.74095
76.65673	77.01796	76.71349	76.39003	76.8294	76.50833
76.24726	76.53071	76.35385	76.35305	76.57197	76.29713
76.27685	76.5684	76.44655	76.24848	76.43765	76.38899
76.50138	76.82499	76.35842	76.22158	76.3273	76.41141

Table B-7: Temperature averages at 1.5 bar, λ_{H_2} =1.2, λ_{O_2} =3.0, 0.10 A/cm^2

75.28352	75.25417	75.20631	74.86766	74.88873	74.83249
75.08923	75.31213	75.19954	74.86343	74.69016	74.66209
74.96163	75.08332	74.95462	74.58357	74.70941	74.31004
74.76661	74.88934	74.80674	74.7646	74.70214	74.28396
74.96258	75.21134	75.18701	74.98991	75.01441	74.83584
75.53126	75.88787	75.50321	75.36795	75.31717	75.246

Table B-8: Temperature averages at 1.5 bar, λ_{H_2} =1.2, λ_{O_2} =3.0, 0.50 A/cm^2

75.93994	75.90137	75.80768	75.36253	75.43213	75.38608
75.96569	76.20267	75.94075	75.46104	75.35421	75.32499
75.80977	75.91877	75.66293	75.21695	75.45371	75.08671
75.51664	75.64	75.47068	75.35698	75.39919	75.02628
75.53892	75.78834	75.72616	75.46702	75.54561	75.41564
75.9454	76.28048	75.85584	75.68922	75.68143	75.66569

Table B-9: Temperature averages at 1.5 bar, λ_{H_2} =1.2, λ_{O_2} =3.0, 0.90 A/cm^2

76.9822	76.98223	76.81231	76.35014	76.51254	76.46018
77.18401	77.52602	77.13986	76.61333	76.63825	76.56319
76.91136	77.11821	76.71601	76.28892	76.70436	76.40434
76.47018	76.65184	76.36192	76.27182	76.47007	76.2202
76.31614	76.59005	76.44804	76.19736	76.39804	76.36879
76.51945	76.84132	76.38059	76.23357	76.31606	76.40805

Table B-10: Temperature averages at 1.5 bar, λ_{H2} =2.0, λ_{O2} =3.0, 0.10 A/cm^2

75.07259	75.0241	75.02939	74.67621	74.71274	74.62171
74.9209	75.16527	75.05173	74.65861	74.50199	74.46436
74.78385	74.91136	74.75772	74.38352	74.51098	74.10508
74.57373	74.69127	74.61303	74.54309	74.49383	74.0629
74.77817	75.03587	74.99259	74.77892	74.80178	74.60372
75.33659	75.7277	75.32524	75.15881	75.09247	74.99117

Table B-11: Temperature averages at 1.5 bar, λ_{H2} =2.0, λ_{O2} =3.0, 0.50 A/cm^2

75.93608	75.89671	75.79889	75.41264	75.51437	75.42634
75.90462	76.17877	75.9171	75.49442	75.419	75.35811
75.71367	75.84806	75.59172	75.18476	75.41309	75.03392
75.3976	75.53156	75.36293	75.27007	75.31369	74.94534
75.42148	75.69833	75.63295	75.39353	75.47639	75.3428
75.86395	76.22788	75.79439	75.62544	75.62999	75.60739

Table B-12: Temperature averages at 1.5 bar, λ_{H2} =2.0, λ_{O2} =3.0, 0.90 A/cm^2

76.94841	76.90632	76.71444	76.29342	76.48937	76.43579
77.08508	77.35635	76.9729	76.5049	76.56242	76.5084
76.79123	76.91718	76.50907	76.10162	76.51722	76.22857
76.30658	76.42915	76.1466	76.05361	76.25117	76.03026
76.12611	76.38647	76.25237	76.00791	76.18759	76.15064
76.31718	76.65494	76.19223	76.0307	76.11916	76.20775

Appendix C: Linearized Graphs for Other Stoichiometric Factors

Figure C-1: Linearized graph of unfolded data for λ_{H2} =1.2, λ_{O2} =2.5, 0.10 A/cm^2

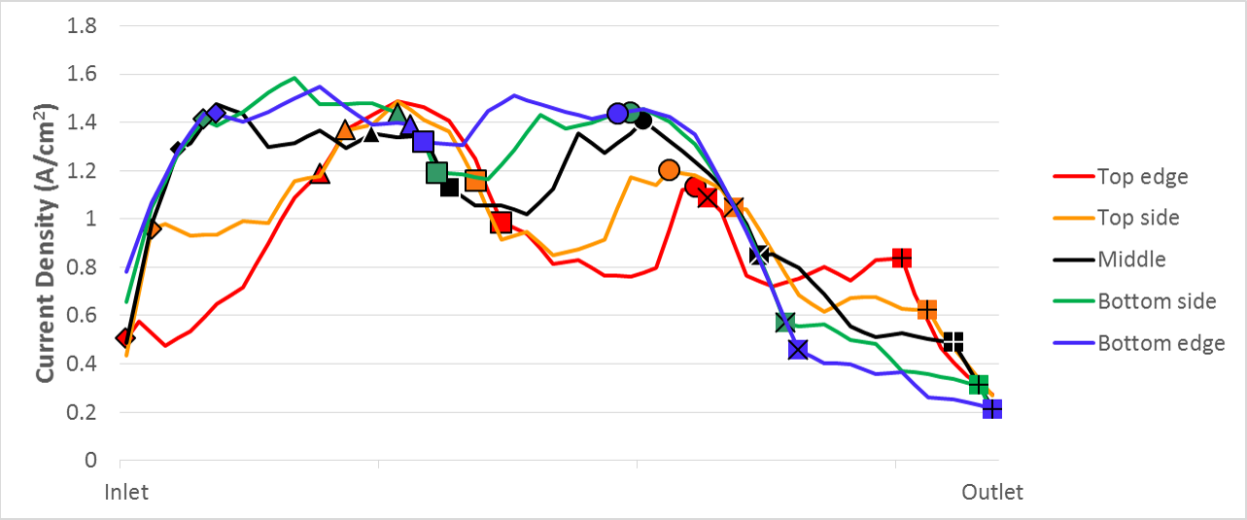

Figure C-2: Linearized graph of unfolded data for λ_{H2} =1.2, λ_{O2} =2.5, 0.50 A/cm^2

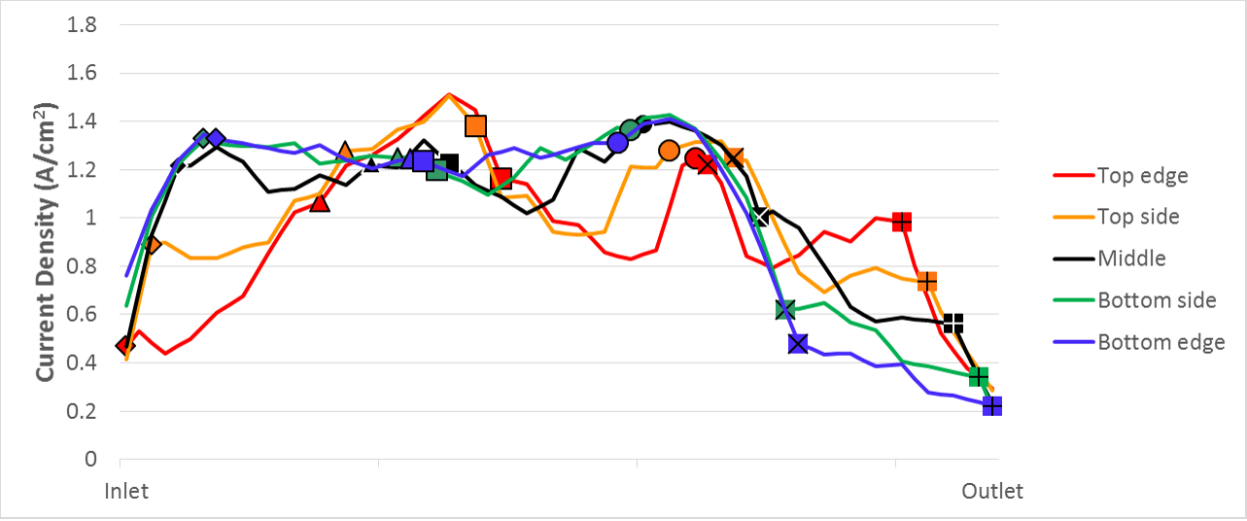

Figure C-3: Linearized graph of unfolded data for λ_{H2} =1.2, λ_{O2} =2.5, 0.90 A/cm^2

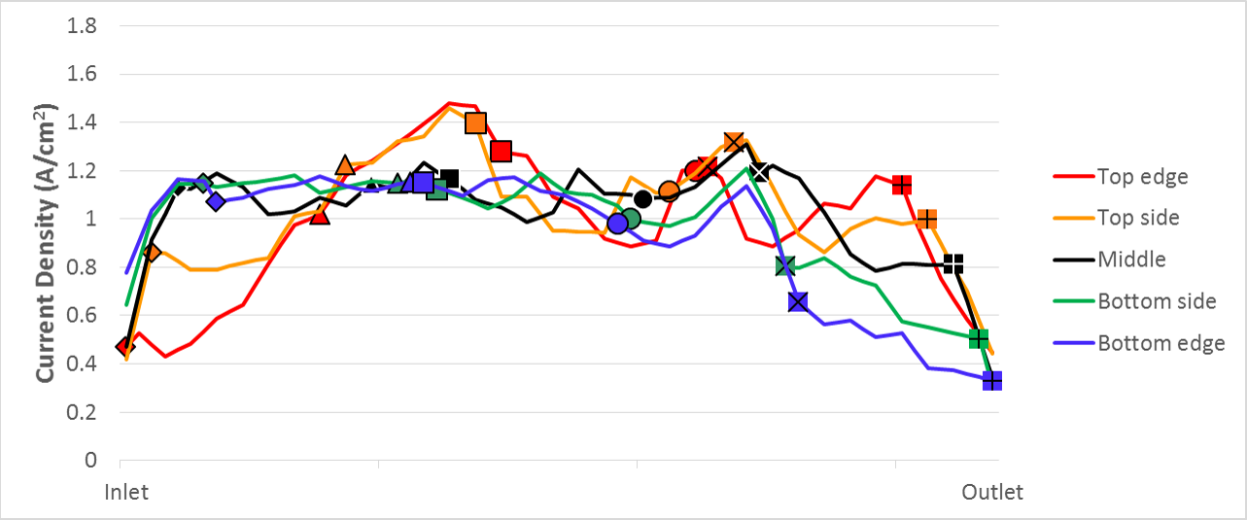

Figure C-4: Linearized graph of unfolded data for λ_{H2} =1.2, λ_{O2} =3.0, 0.10 A/cm^2

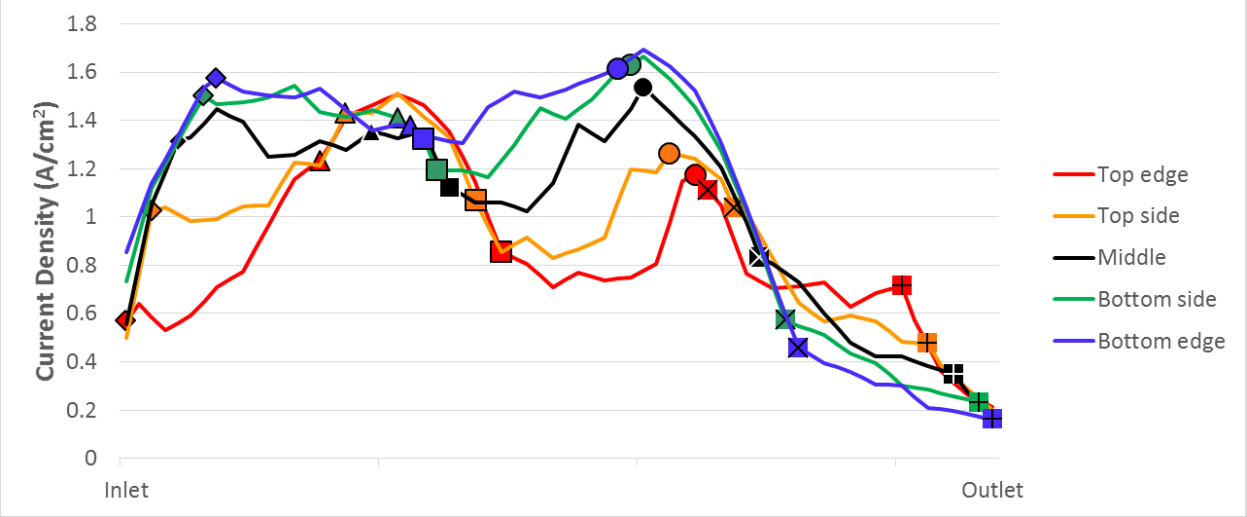

Figure C-5: Linearized graph of unfolded data for λ_{H2} =1.2, λ_{O2} =3.0, 0.50 A/cm^2

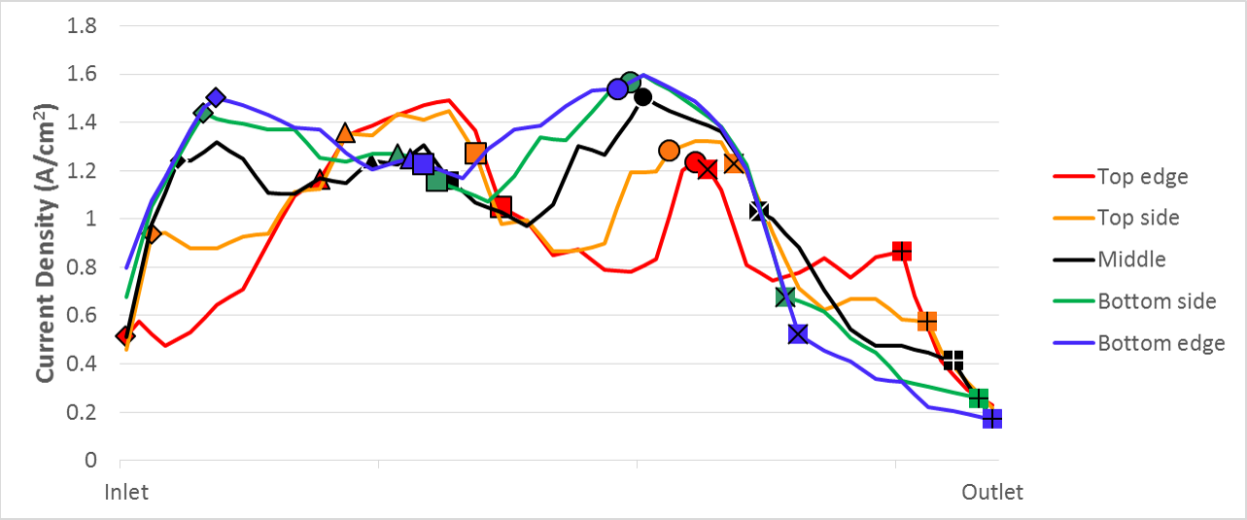

Figure C-6: Linearized graph of unfolded data for λ_{H2} =1.2, λ_{O2} =3.0, 0.90 A/cm^2

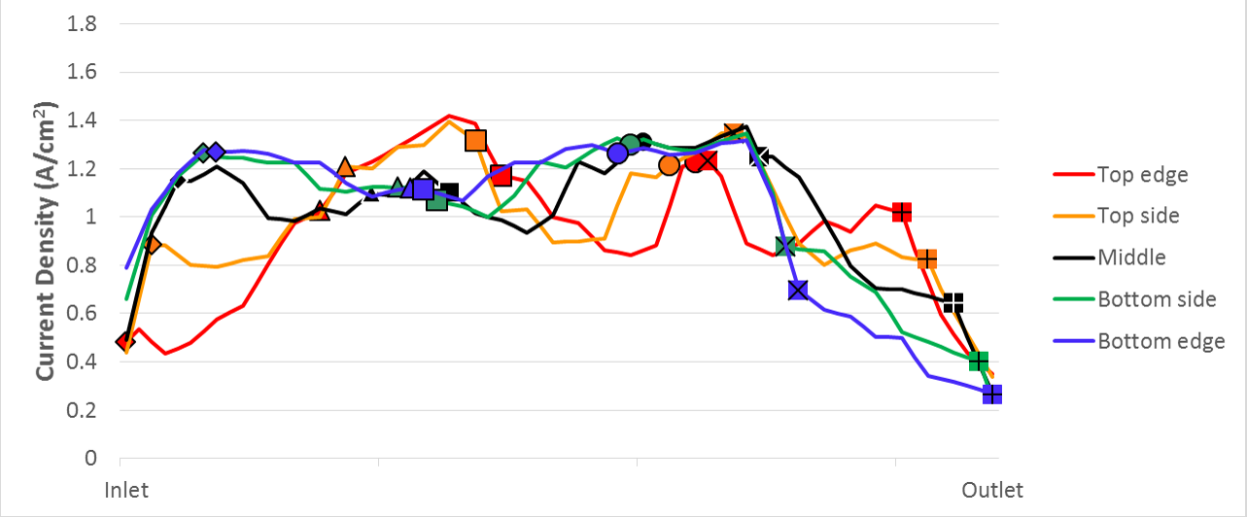

Figure C-7: Linearized graph of unfolded data for λ_{H2} =2.0, λ_{O2} =3.0, 0.10 A/cm^2

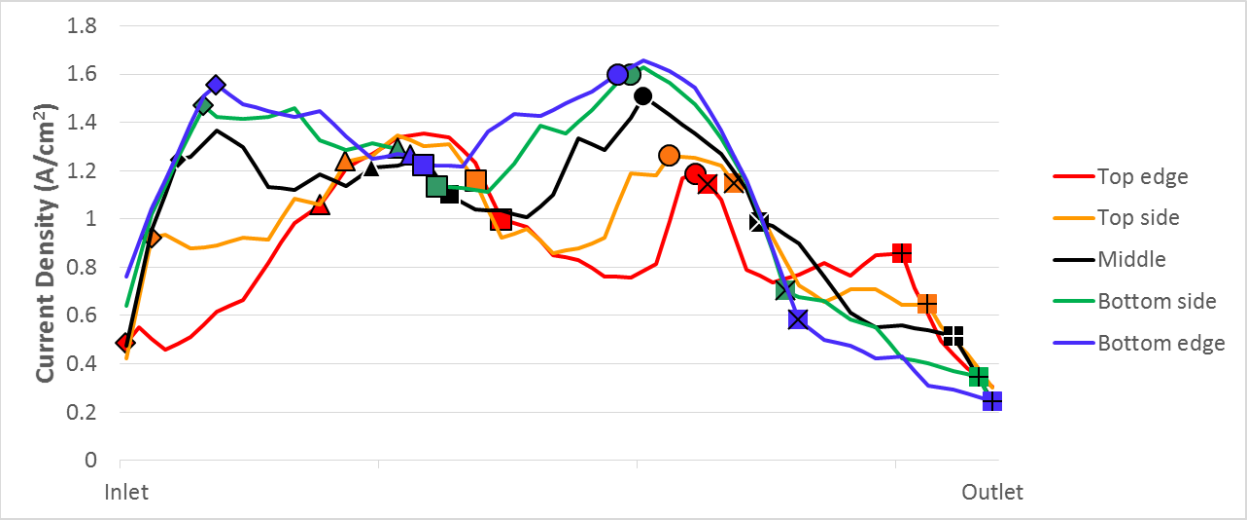

Figure C-8: Linearized graph of unfolded data for λ_{H2} =2.0, λ_{O2} =3.0, 0.50 A/cm^2

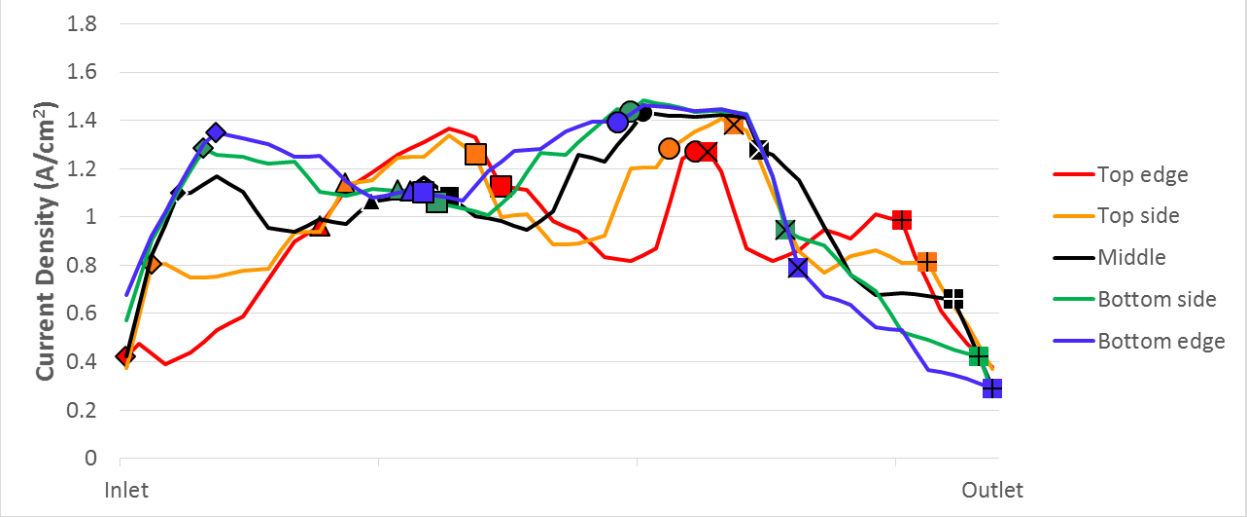

Figure C-9: Linearized graph of unfolded data for λ_{H2} =2.0, λ_{O2} =3.0, 0.90 A/cm^2